Model for the Formation of Longshore Sand Ridges on the Continental Shelf

Juan Mario Restrepo

Mathematics and Computer Science Division

Argonne National Laboratory, Argonne, IL U.S.A. 60438

Jerry L. Bona

Mathematics Department

The Pennsylvania State University, University Park, PA U.S.A. 16802

January 5, 1994

Abstract

A model is proposed for the formation and evolution of three-dimensional sedimentary structures such as longshore sand ridges on the continental shelf in water deeper than that of the shoaling region. Owing to the striking similarity between the bar spacing and the length scales in which interactions among the most energetic modes of shallow water waves take place, we argue that these bars are formed slowly by flows in the turbulent boundary layer generated by weakly nonlinear, dispersive waves. Hence the model is based on the interaction between surficial, weakly nonlinear shallow water waves, having weak spanwise spatial dependence, and the bottom topography.

While such underwater structures are not the result of a single formative agent, it is argued that the mechanism proposed in this study does contribute significantly to their generation and evolution. Comparisons of this model with oceanographic data must wait for sufficient data to become available. In conjunction with developing the sand ridge model, this study proposes new mathematical equations of interest in their own right.

Contents

1 Introduction

The dynamics of sand ridges are not well understood. Sand ridges are underwater barlike features of the continental shelf, composed of loose granular sediment. Hundreds of meters long and up to a few meters high, sand ridges are usually found in groups, arranged in more or less parallel rows separated from each other

by hundreds of meters. They may be loosely classified as either tidal ridges or longshore sand ridges. Tidal ridges are oriented parallel to the prevailing direction of the local ocean currents, whereas longshore sand ridges are oriented normal to the direction in which the overlying water waves propagate. In this study we propose a possible mechanism for the formation and evolution of longshore sand ridges.

It deserves emphasis that the often complex seabed structures appearing off many continental coasts are likely to owe their existence to a multitude of causes. We introduce here a very simple, wave-generated mechanism that does provide a dynamical model of wave-bottom interaction leading to the formation of barlike structures in suitable oceanographic environments. It is not suggested that the intentionally crude model can account for everything we observe. The model is constructed in such a way, however, that it can be implemented using data that is sometimes available from field studies, and without introducing adjustable parameters.

The plan of this paper is as follows. In this introduction, a précis is provided of the morphology of oceanic sedimentary structures; observational and laboratory research in this area is briefly reviewed, and various sedimentation and sandbar models are outlined. The equations describing the evolution of the water waves are covered in Section 2. Section 3 deals with the wave-driven boundary layer and with a consequent mass transport equation. To give a qualitative idea of the behavior of solutions to the model, we present in Section 4 several numerical simulations. Section 5 reviews the preceding sections and lists open questions worthy of future pursuit.

1.1 Morphology of Oceanic Sedimentary Structures

Until recently, it was thought that sand ripples, like those found in the beach zone, and their larger cousins the sandbars and sand ridges were morphologically similar. We now recognize a variety of different sedimentary structures, defining the categories by shape or generating mechanism. Examples are sand ripples, ridge-runnel systems, tidal ridges, and longshore sand ridges.

In the near-beach zone, including the breaker zone, occur small sand ripples on the order of a few centimeters high, which come in a multitude of shapes and forms. Larger structures, such as crescentic bars, occur as well. In this region the fluid flow is quite complex, since there are both incident and reflected waves, tidal flow effects, and turbulence and entrainment of air from wave breaking.

The ridge-runnel system, so common in the near-beach zones in the American Northeast and in the Great Lakes [1], is composed of a large bump 3 to 15 meters away from the beach, about 0.3 meters high and up to perhaps 7 to 10 meters in length, which is preceded by a runnel. The runnel may or may not be scoured with small ripples. The system is thought to be formed by storms eroding the beach and the dune fields and/or by tidal currents [1]. Davis et al. [1] provide observational evidence for their claim that storms seem to play a minor role in the evolution of these structures once they have formed.

Tidal ridges, which were noticed by Off [2], are rhythmic features oriented parallel to the direction of tidal currents. They are 8 to 30 meters high, 7 to 60 kilometers long, and spaced 1 to 10 kilometers apart. Allen [3] found that their height is roughly proportional to the square root of their spacing and that they are

composed of sand, silt, and mud. He reported that they occur where tidal currents reach at least 2 to 7 km/h and where there is an ample supply of sediment. Tidal ridges are also prominent in the neighborhood of river deltas. Tidal ridges may have a fairly flat dome, suggesting to some researchers that erosion effects play a very minor role.

Sandbars are distributed in complicated patterns on the continental shelf, and it is sometimes difficult to discern which is a tidal ridge and which is a longshore sand ridge, the object of attention in this study. For example, Figure 1 taken from a paper by Swift [4] shows the relative orientation of different types of ridges. Note that some bars fan out around river deltas, while some are oriented parallel to or almost normal to the coast.

Longshore sand ridges are common features of the continental shelf in water deeper than the surf zone, from the near-shore region to the farthest reaches of the shelf. The better-known ridge fields are those found in the shallowest end of this range, primarily because they are readily seen, as illustrated in Figure 2, which shows the bar system off central Harrison County, Mississippi. Other near-shore systems are found along the coasts of the Carolinas, Florida, the northern coast of Alaska, the Black Sea, the Baltic Sea, and even large lakes such as Lake Michigan. Longshore sand ridges can also be found in the farthest reaches of the shelf hugging every continent around the world. Observations seem to indicate that a mean slope in the neighborhood of 0.02 to 0.05 favors the formation of longshore sand ridges [5]. Such ridges are composed mostly of fine sand and silt, sometimes of mud. The mean sediment particle size ranges between 0.1 and 0.5 millimeters. Groups of up to 12 ridges have been found that are more or less parallel to each other.

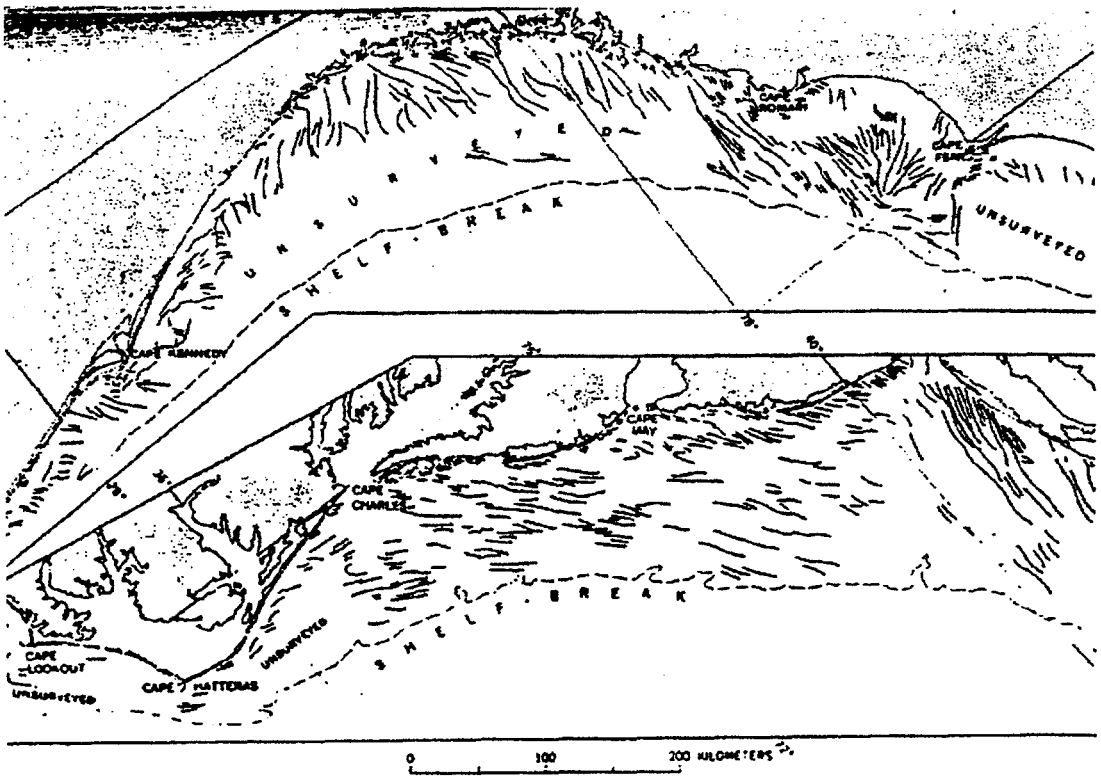

Figure 1: Submerged ridge field from Long Island to Florida, from Swift [4]

Some ridge fields are observed to change position over time. Their migration rates vary from place to place; for instance, the ridges on Sable Island Bank have been estimated to move at rates ranging from 0.5 meters per year, in water 60 meters deep, to 5 meters per year, in 30-meter depths [6]. Ridge fields are routinely found in regions where the water depth is small compared with the wavelength of an overlying internal wave environment with frequencies in the infragravity range [7].

It is clear that the formation and maintenance of these sedimentary structures are connected with the ambient hydrodynamics. One possibility is that ridges are generated by major events such as storms, while another prospect is that they

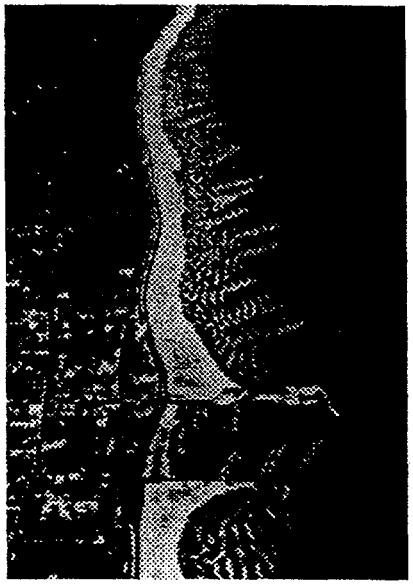

Figure 2: Sand ridges in shallow water, Harrison County, Mississippi

come about as a result of systematic aspects of the surrounding fluid flows. Lau and Travis [5] found that sandbars beyond the breaker zone do not disappear but simply change location after a severe storm. Short, in his field observations in Northern Alaska [7], found that severe storms seem to rework the bars, but that some sandbars photographed in 1949 and 1955 were still identifiable after approximately 30 years. Preliminary data from the so-called Super Duck [8] experiments show this bar "reworking" as a consequence of major storms. Other evidence points in the same direction and inclines one to the view that systematic aspects of the hydrodynamic environment play a decisive role in ridge generation. A related question is whether wave breaking is an essential ingredient in the generative processes leading to sand ridges. While categorical evidence does not present itself, it is true that sand ripples form in a laboratory flume under the action of waves and that sand ridges appear in regions where there is no apparent breaking. Both the

above points will figure in the mathematical conceptualization of the situation to be presented in this paper.

Several significant differences exist in the near and far ends of the continental shelf insofar as the fluid environment is concerned. First, in the near-shore zone, strong incident and reflected components to the wave field may be identified. Second, the effect of wind stresses on the boundary layer flows is quite significant in the nearshore. Third, while significant asymmetry exists in the velocity field in both areas, quite pronounced asymmetry can occur in the acceleration field in the nearshore case. Bijker et al. [9] made laboratory measurements of acceleration and velocity fields for water waves with fairly high Stokes numbers, in the range of 12–57. They found the net transport to be in the direction of the wave, particularly if the wave was very nonlinear. Smaller particles seemed to be transported mostly by the Stokes flow, whereas larger particles responded in the main to the "acceleration" field. Hallermeier [10] analyzed a large experimental data set and found an empirical rule for the prediction of ripple characteristics based on the acceleration field, which suggests that this field may be an important sand-transport mechanism in the near-beach zone. Elgar et al. [11] made measurements in the shoaling region, in water depths in the range of 1–6 meters, over a topography with mean slope of 5%, and confirmed in the field the existence of the velocity and acceleration field asymmetry. They found that the acceleration asymmetry becomes increasingly significant with decreasing water depth. These investigations suggest that the acceleration field becomes ever more important as the distance to the beach decreases; our model would not apply in this area, since the adopted transport equation does not include acceleration effects.

1.2 Sediment-Transport Models

As mentioned, much of the work on sedimentation has been aimed at understanding how the sediment moves, rather than how it generates patterns. Most researchers working on sediment transport assume an outer fluid flow at the edge of a boundary layer and attempt to model sediment motion on the bed and in the boundary layer. Sleath [12] presents a good review of the subject, and we therefore content ourselves with a cursory summary of the various sedimentation models.

A model developed by Bagnold [13,14] assumed that wave-induced oscillatory water motion causes sediment to move back and forth with a net expenditure of energy. Although no net transport results in such an oscillatory flow, the energy dissipation acts to keep the sediment in suspension. Once in suspension, any steady current superimposed on this oscillatory flow will then cause a net transport of the suspended sediment in the direction of the instantaneous total bottom stress. Originally a bed-load model, Bagnold's model has also been applied to suspended-load transport for low Froude number flows. A threshold of motion parameter called the Shield's parameter is incorporated into the model to reflect the fact that a critical amount of energy must be imparted on the bed before transport can occur. Smith [15] and Fredsœ [16] applied this model to the ocean environment. They assumed a constant eddy viscosity and obtained criteria for the onset of instability and ripple formation. Richards [17] used instead a turbulent scale that increases linearly in height from the bed, thus obtaining two modes of instability that yield small- and large-scale ripples, respectively. Bagnold's model has also

been used with some success in the near-shore zone, in a version that includes the effect of wind on sediment transport rate [18]. However, Bailard and Inman [14] found that the model did not perform adequately when the waves are not normally incident to the beach.

Another sedimentation model by Raudkivi [19] and by Williams and Kemp [20] attributes the formation of ripples to a chance piling of sediment. This deformation then causes the flow to separate, with subsequent building up of the ripple downstream. They attribute the initial small deformation to the random action of highly turbulent velocities, or "bursts," close to the bed.

Last, we mention the model in the Longuett-Higgins paper [21]. He showed how a second-order drift velocity, which was first noted by Stokes [22], develops in the boundary layer from an outer linear oscillatory flow or in the bulk of the fluid through the action of nonlinear waves. This drift velocity is capable of transporting sediment, particularly suspended sediment. A number of people have studied this mechanism; of note are Johns [23], who developed explicit expressions appropriate for the ocean environment and studied the character of the drift velocity and its stability, and Blondeaux [24] and Vittori and Blondeaux [25], who looked at the stability and formation for Froude numbers at which flow separation does not occur. They determined adequate height, spacing, and onset thresholds, by comparison with laboratory experiments. The second of these papers introduced more structure and made a case for the inclusion of nonlinear effects in the flow immediately outside of the boundary layer.

1.3 Sedimentary Bar Models

Among the researchers who have coupled a sedimentation transport model to an oceanic wave field to look at the process of bar formation in the oceanic environment are Holman and Bowen [26]. They use the fully three-dimensional, linearized water wave equations to compute the drift velocity, which in turn they couple to Bagnold's transport model for suspended load. In particular, they examine the edge-wave case in an effort to compute the formation of crescentic bars in the shoaling region. Bowen [27] has also examined the performance of this model in predicting the spacing of longshore ridges and reports good qualitative agreement with field observations.

Laboratory and field observations indicate that standing wave patterns display a Bragg resonance process with an underlying wavy bottom [28] [29]. In a steady-state situation, the ripples develop a spacing that is roughly half the local average length of the water waves. This first-order theory [28,30–32] is applicable in principle to the near-shore environment, since it relies on the scouring effect of a standing wave pattern. It has been widely studied since it is easily implemented in the laboratory; at one or another time, various researchers have implicated this mechanism as the general reason we observe stable sandbars in the near-shore area.

The ridge and runnel system have been modeled with a variant of Bagnold's transport formula by Dean [18] and deVriend [33]. The extent of the model's success is somewhat difficult to discern, however. Since the undertow and the local bed slope are significant and since the effect of the wind in generating stresses on the surface of the ocean must be taken into account, modeling the formation of

runnels is very difficult. Russell and Osorio [34] and Bijker et al. [35] found that on a sloping beach, the mass transport velocity near the bed was onshore before breaking and offshore after. This effect, which seems to be independent of wave reflection from the beach, may explain why these bar systems are usually found close to the plunge line of breakers.

Huthnance [36] developed a theory for the formation of tidal ridges based on an instability that is triggered by a small protuberance on the shelf. The ensuing boundary layer develops a bar that is fed by bedload. The resulting steady-state bar is finite in extent and parallel to the assumed, always-present currents. Equilibrium is reached when the supply of sand is exhausted. Huthnance notds that the tops of these ridges are flat rather than rounded, which he claimed dismisses erosion as being the source for the generation of these structures. Huthnance's study does not address the periodic nature of these bars, nor does it suggest a relation between their height and spacing.

Among the first to suggest that infragravity standing waves may be responsible for longshore sand ridge formation was Suhaida [37]. He did so at a time when few people saw anything fundamentally different about near-shore sandbars where a strong standing-wave field may be present, and bars or ridges far from the beach where little or no standing wave pattern is to be found. Short [7], in field measurements of sand ridges in Alaska, found a loose correlation between the ridge spacing and the average peak infragravity component wavelenth.

Lau and Travis [5] derived a drift velocity from a Stokes water-wave field for a bed with constant slope. Their model yields the spacing and the number of ridges from the periodicity of the drift velocity. They made use of the SRIT (slightly res-

onant interacting triads) approximation developed by Lau and Barcilon [38] and Mei and Ümlüata [30] for weakly nonlinear shallow-water waves to solve approximately for the wave motion.

Boczar-Karakiewicz conducted a number of interesting field and laboratory studies [28] [39]. The an analysis of her findings [40], she combined the hydrodynamic approximation of Lau and Barcilon with the boundary-layer theory of Longuett-Higgins [21]. Exploiting the large discrepancy between the time scales relevant to wave propagation and sediment dynamics, these investigators formulated the first evolutionary models for sand ridge formation. The original model is appropriate in principle for the shallower end of the continental shelf since it was derived for an isotropic water environment. Later, the model was extended to take account of internal waves and this version was tested against actual field data [41]. Encouraged by the outcome of the comparisons with field data, we have extended the model's applicability to three dimensions.

Referring to Figure 3, we envision infragravity waves coming into the purview of the model at the line $x = 0$, which is determined in relatively deep water as the location where the waves begin to be significantly influenced by the bottom topography. The x direction increases as the wave travels shoreward. The spanwise direction, which is the y coordinate in our reference frame is approximately parallel to the line of constant phase of the incoming waves. The waves propagate shoreward, possibly at an angle with respect to the prevailing direction of maximum gradient of the bottom topography. In the deeper reaches of the shelf. the drift velocity is produced by waves supported by the picnocline, while in the

shallower end of the ocean where the water column is more isotropic, the drift velocity is a boundary layer manifestation of the waves on the ocean surface. The extent of the model is limited in the shoreward direction by the disintegration of the interface supporting the internal waves, by the approach to the breaking zone for surface waves, by any singularity in the depth, or by significant energy transfer from low to high frequencies that are ignored by the hydrodynamic modeling. The spanwise direction is limited by the same sort of issues. Taking advantage of the disparate time scales for bottom and fluid evolution, we assume that the gently sloping bottom is fixed in the time span in which the water wave begins its trip towards the shore, progresses, and eventually dissipates in the shallow end of the model's purview. Taking advantage of this assumption, we can then decouple the problem: starting with some initial bottom configuration, we can obtain the hydrodynamics of the water surface, which evolves on a time scale t, say. This in turn yields the drift velocity in the boundary layer; the resultant drift velocity is then used in a transport equation to update the bottom topography, which is evolving on a time scale T that is considerably longer than t.

A few comments are deserved about the general mechanism for longshore ripple and sand ridge formation. If a standing-wave pattern exists in the surface waves, whether it be a result of linear or nonlinear effects, the scouring effect of the waves presumably generates ripples obeying a Bragg scattering mechanism (see [28]). This is a first-order phenomenon whose effectiveness in influencing the shape of the bottom topography relies on the existence of both a reflected and an incident wave. Generally, the reflected component becomes weaker and weaker the further it travels seaward. Yet, far from the shore there are abundant fields of large-scale

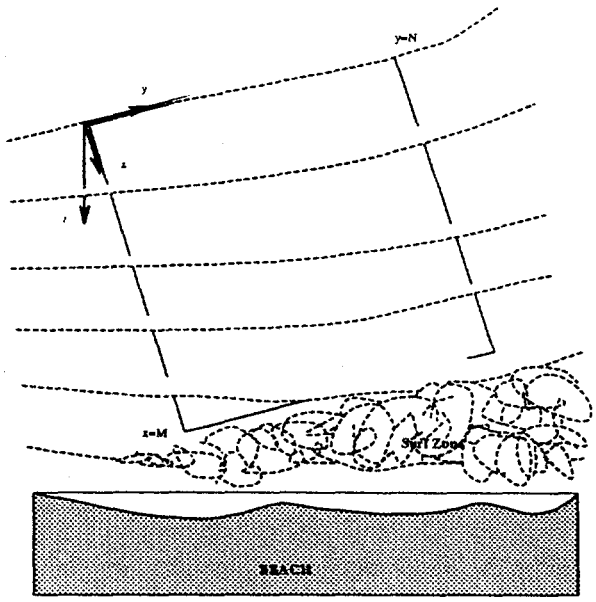

Figure 3: Plan view of the problem

bars. In this deeper region it is suggested that the Bragg mechanism gives way to the second-order, strictly nonlinear theory that is presented in this study. Thus, we envision that both mechanisms operate along the continental shelf; but in the very near-shore reaches, the first-order theory is prevalent, while in the deeper reaches, the second-order theory prevails.

The second-order drift velocity is not exclusively the result of progressive waves incident on the shore. Reflected waves may also contribute. For very mild slopes and relatively large distances from the shore, however, the reflected component is sometimes quite weak. This issue wil be discussed again later.

2 Hydrodynamics of the Water-Wave Problem

A striking similarity exists between the typical bar spacing and the length scale at which energetic interactions among the most significant modes of shallow-water waves takes place. Hence, it is suggested that longshore sand ridges are formed by flows in the boundary layer that are generated by these weakly nonlinear long water waves. The goal in the present section is to develop a crude but useful model for the important aspects of the overlying hydrodynamics on the surface and in the body of the fluid. The interaction of the flow environment with the sediment in a boundary layer at the bottom of the fluid column is treated in Section 3.

Figure 4 is an illustration of the hydrodynamic problem. The free surface is given by $z = \eta(\mathbf{x}, t)$ and the bottom by $z = -H(\mathbf{x}, T)$, where the notation $\mathbf{x} = (x, y)$ is used to denote the transverse coordinates. A thin boundary layer of thickness δ hugs the bottom topography. The spatial domain for the hydrodynamic problem is $\Omega_T = \mathbf{R}^2 \times [-H(T) + \delta, \eta(t)] \approx \mathbf{R}^2 \times [-H(T), \eta(t)]$, since $\delta \ll |H|$. The T is used to remind us that the scale of time evolution of the bottom is different from that of the fluid environment; hence, it appears here as a parameter. The fluid is subjected solely to gravitational forcing.

The following introduces the notation to be used throughout this study. The velocity field is given by $(\mathbf{u}, w)$, where the first entry is the transverse velocity (u, v) and w is the vertical velocity. Position is represented by the vector $(\mathbf{x}, z)$. The standard three-component gradient operator is explicitly split into its transverse and vertical coordinates, so that $\nabla_3 \equiv \nabla + \hat{z}\partial_z$. The same convention is followed for the Laplacian operator Δ_3. Incompressibility and irrotationality are assumed

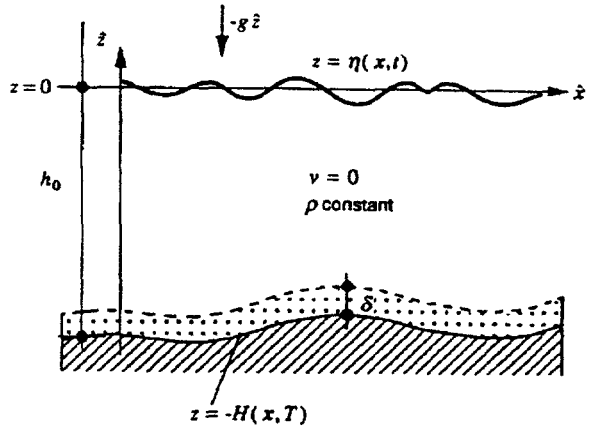

Figure 4: Side view, surface wave problem

to hold in the bulk of the fluid, and its viscosity is assumed negligible in Ω_T. The bottom is taken to be impermeable which together with no-slip conditions for the fluid/bottom interface leads to

$$\phi_z = -\nabla H \cdot \nabla \phi, \text{ at } z = -H, \tag{1}$$

where

$$(\mathbf{u}, w) = \nabla_3 \phi. \tag{2}$$

Because of the continuity equation, the velocity potential ϕ is harmonic in the flow domain, which is to say

$$\Delta_3 \phi = 0, \text{ in } \Omega_T. \tag{3}$$

At the air-water interface, conservation of momentum requires the pressure to be continuous. The assumed constant value of the pressure immediately above the water is set to zero. Hence, the pressure at the interface when the surface

is quiescent is zero. Furthermore, a kinematic condition on the interface leads to $\phi_z = \eta_t + \nabla\phi \cdot \nabla\eta$ at $z = \eta$.

2.1 Hamiltonian Formulation of the Hydrodynamic Problem

In this subsection, a useful Hamiltonian formulation of the hydrodynamic problem is proposed. This aspect relies heavily on ideas developed by Zakharov and Shabhat [42], Miles [43], Bowman [44], and especially Benjamin [review stability benjamin] and Benjamin and Olver [benjamin olver].

To begin, we note that the motion of the entire fluid body can be determined once the free surface motion is known. Specifically, if the function η that describes the free surface, and the velocity potential at the free surface, $\Phi \equiv \phi(\mathbf{x}, z = \eta, t)$, are known, then Ω_T is determined by η and ϕ is determined by the condition $\phi = \Phi$ at the free surface, together with the boundary condition at the bottom, the fact that ϕ is harmonic in Ω_T, and the asymptotic conditions $|\nabla_3\phi| \to 0$ as $|\mathbf{r}| \to \infty$.

Consider the Hamiltonian $E = E(\eta, \Phi)$. The choice of label E reflects the fact that the Hamiltonian for this problem is conserved and is numerically equal to the sum of the potential energy V and the the kinetic energy K. As shown by Benjamin and Olver [45], the evolution of the free surface is given by the Hamiltonian system

$$\begin{aligned} \eta_t &= \frac{\delta E}{\delta \Phi} \\ \Phi_t &= -\frac{\delta E}{\delta \eta}, \end{aligned} \tag{4}$$

where E is the Hamiltonian.

We specialize Equation (4) for the case of weakly nonlinear shallow-water waves. Define the parameters $\alpha \ll 1$ and $\beta \ll 1$, where α is characteristic of the size of the nonlinearities and β^2 characteristic of the degree of dispersiveness of the surface waves. In terms of physically relevant parameters, $\alpha = a/h_0$ and $\beta = h_0/\lambda$, where a is the typical wave height, h_0 the characteristic of the fluid column size, and λ the typical length of the water waves. Further, it is assumed that $O(\alpha) \sim O(\beta^2)$. The Stokes number S, which is a measure of the balance between nonlinear to dispersive effects, is defined as the ratio α/β^2. For $S \ll 1$, nonlinear effects are weak, and only a small portion of energy transfer occurs on moderate space-time scales, so that O(1) nonlinear effects are possible only after very large scales. For $S \sim 1$, inertial effects are of the same order as dispersive effects. In view of this, we take $\eta = O(\alpha)$, $\Phi = O(\alpha)$, and the differentiations $\partial_z, \partial_t, \nabla = O(\beta)$. We defer the description of the bottom topography to a later stage, but for now assume that $H = O(1)$, $\nabla H = O(\alpha)$,

An approximation to ϕ, which satisfies the boundary value problem, is

$$\begin{array}{rcccc} \phi(\mathbf{r},z,t) = & \Phi(\mathbf{r},t) & - & \frac{1}{2}z^2\nabla^2\Phi(\mathbf{r},t) & - & z\nabla\cdot(H\nabla\Phi(\mathbf{r},t)) \\ & O(\alpha) & & O(\alpha\beta^2) & & O(\alpha\beta^2) \end{array}$$

which can be easily derived using Rayleigh's trick [46]. The gradient of the above expression

$$\mathbf{U}(\mathbf{r},z,t) = \mathbf{u}(\mathbf{r},t) - \{z\nabla[\nabla\cdot(H\mathbf{u}(\mathbf{r},t))] + \frac{1}{2}z^2\nabla(\nabla\cdot\mathbf{u}(\mathbf{r},t))\} \tag{5}$$

gives the velocity anywhere in the inviscid domain of the fluid.

The potential energy is exactly

$$V = \int_{\mathbf{R}^2} d^2r \frac{1}{2} g\eta^2. \tag{6}$$

The kinetic energy is calculated by using the approximation developed above for the velocity potential, Equation (5):

$$K = \int_{\mathbf{R}^2} d^2r \{\frac{1}{2}(H+\eta)(\nabla\Phi)^2 + \frac{H}{2}(\nabla H\cdot\nabla\Phi)^2 - \frac{H^3}{6}(\nabla^2\Phi)^2\}, \tag{7}$$

which is an expression of $O(\alpha^3\beta^2)$, and $O(\alpha^2\beta^4)$.

Thus, in terms of the velocity at the surface $\mathbf{u} \equiv \nabla\Phi$ and the displacement, the energy is

$$E = V + K_0 + \alpha K_1 + \cdots, \tag{8}$$

where

$$K_0 = \int_{\mathbf{R}^2} d^2r \frac{1}{2} H\mathbf{u}^2 \tag{9}$$

$$K_1 = \int_{\mathbf{R}^2} d^2r \{\frac{1}{2}\eta\mathbf{u}^2 + \frac{H}{2}(\nabla H\cdot\mathbf{u})^2 - \frac{H^3}{6}(\nabla\cdot\mathbf{u})^2\}, \tag{10}$$

and V is as before. Substituting E in Equation (4), to lowest order, yields the wave equation

$$\eta_t + \nabla\cdot(H\mathbf{u}) = 0 \tag{11}$$

$$\mathbf{u}_t + g\nabla\eta = 0. \tag{12}$$

To the next order,

$$\eta_t + \nabla\cdot[(H+\eta)\mathbf{u}] + \nabla\cdot[\mathbf{u}\nabla(H^2)\cdot\nabla H + \frac{1}{3}\nabla(H^3\nabla\cdot\mathbf{u})] = 0 \tag{13}$$

$$\mathbf{u}_t + (\mathbf{u}\cdot\nabla)\mathbf{u} + g\nabla\eta = 0, \tag{14}$$

a version of a Boussinesq system [47]. The Boussinesq system (BSS) is a shallow-water, long-wavelength, weakly nonlinear approximation to the Euler equation which admits bidirectional waves as solutions. The version given by Equations (13) and (14), however, has a couple of troublesome characteristics from the standpoint of modelling a physical situation. Specifically, the system is linearly unstable and rather poor at conveying accurately the full dispersion relation [48]. The instability can be shown by the substitution of plane wave solutions into the linearized version of Equation (14), and the degree to which the equation's dispersion relation differs appreciably from the full-water wave dispersion is most apparent for the higher wavenumber. By making changes in the dispersive term (i.e., regularizing), it is possible to overcome the instability problem and improve the agreement between the full dispersion relation and the long wave limit.

The BSS is regularized by exploiting the specific form of the bottom topography. Using Equation (12), and the fact that $\nabla H = O(\alpha)$, we approximate

$$\nabla\cdot[\mathbf{u}\nabla(H^2)\cdot\nabla H + \frac{1}{3}\nabla(H^3\nabla\cdot\mathbf{u})] = -\frac{1}{3}\nabla\cdot[\nabla(H^2\eta_t)] + O(\alpha). \tag{15}$$

Thus, the regularized system (RB) adopted in this study, as an approximate model for the water waves, is

$$\eta_t + \nabla\cdot[(H+\eta)\mathbf{u}] - \frac{1}{3}\nabla\cdot[\nabla(H^2\eta_t)] = 0 \tag{16}$$

$$\mathbf{u}_t + (\mathbf{u}\cdot\nabla)\mathbf{u} + g\nabla\eta = 0. \tag{17}$$

Since the velocity is in terms of the surface values, rather than in terms of averaged-depth velocity, say, the irrotational condition, with u and v being respectively the shoreward and spanwise velocity components, remains in the simple form

$$u_y = v_x, \tag{18}$$

which is quite convenient in the development of three-dimensional problems.

Using the convention in what follows that *new* $\leftarrow$ *scale* $\times$ *old*, wwe adopt the scaling

$$t \leftarrow \frac{\sqrt{gh_0}}{\lambda}t \quad \mathbf{u} \leftarrow \frac{\sqrt{h_0}}{\sqrt{g}a}\mathbf{u} \quad \eta \leftarrow \eta/a \quad h \leftarrow \frac{H}{h_0} \quad \mathbf{r} \leftarrow \frac{\mathbf{r}}{\lambda} \tag{19}$$

where h_0 is a characteristic depth of the water column.

In addition, the spanwise dependence is scaled to reflect the fact that waves are propagating primarily in the shoreward direction. To do so, we assume that there is a constant $q \ll 1$ such that

$$O(|\,\hat{x}\cdot\mathbf{K}\,|) = q \times O(|\,\hat{y}\cdot\mathbf{K}\,|), \tag{20}$$

for which a consistent uniform expansion of the RB exists and that is physically

relevant. If nonlinear, dispersive, and weak y variation effects are to balance, the size of the constant must be of the order of the reciprocal of β. Since this parameter has considerable nuisance value, the parameter q will be set equal to $1/\beta$ for the rest of this study. This implies that the spanwise variables must be scaled

$$y \leftarrow \alpha^{1/2} y \qquad \hat{y}\cdot\mathbf{u} \leftarrow \alpha^{-1/2}\hat{y}\cdot\mathbf{u}, \tag{21}$$

which will alter the regularized system but will not affect the irrotational condition, Equation (18).

2.2 Description of the Bottom Topography

Laboratory data [28] suggests that there are two time scales: a fast time scale t, which measures the evolution of the fluid quantities, and a slow time scale T, which is characteristic of the evolution of the bottom topography. In addition, the data suggests that the typical height and slopes of the longshore sand ridges are such that $\varepsilon = O(\nabla^n h) = O(\alpha)$. Furthermore, the type of longshore sand ridge under consideration is such that the measure of longshore spatial variation is larger than the spatial variations of the fluid quantities. It is suggested that the sand ridge shoreward variation be $X = \alpha x$. Hence, two scales of shoreward variation exist, so that

$$\partial_x \rightarrow \partial_x + \alpha\partial_X. \tag{22}$$

Thus the bottom in scaled variables is

$$h(X, y, T) = 1 + \varepsilon f(X, y, T), \tag{23}$$

where the function $f = O(1)$.

2.3 Slightly Resonant Interacting Triads (SRIT)

By substituting an expansion of the form

$$\begin{aligned} \eta &= f_0 + \alpha^1 f_1 + \alpha^2 f_2 + \cdots \\ \mathbf{u} &= \mathbf{g}_0 + \alpha^1 \mathbf{g}_1 + \alpha^2 \mathbf{g}_2 + \cdots \end{aligned} \tag{24}$$

into Equations (16), (17), and (18), and matching order by order, it is possible to solve for the surface quantities to lowest orders in α. Our interest is limited to the lowest-order theory. We refer the interested reader to [49] for the details of the higher-order theory.

For the momentum balance, Equation (17), the first two orders in the formal expansion are

$$\begin{aligned} \alpha^0 : \qquad u_{0t} + \eta_{0x} &= 0 \\ v_{0t} + \eta_{0y} &= 0, \\ \alpha^1 : \quad u_{1t} + u_0 u_{0x} + \eta_{1x} + \eta_{0X} &= 0 \\ v_{1t} + u_0 v_{0x} + \eta_{1y} &= 0. \end{aligned} \tag{25}$$

Similarly, (18) yields,

$$\begin{aligned} \alpha^0 : \qquad u_{0y} - v_{0x} &= 0, \\ \alpha^1 : \quad u_{1y} - v_{1x} - v_{0X} &= 0, \end{aligned} \tag{26}$$

at the first two orders. Finally, we derive the relations

$$\begin{aligned} \alpha^0: \quad & \eta_{0t} + u_{0x} - \frac{\beta^2}{3}\eta_{0xxt} = 0, \\ \alpha^1: \quad & \eta_{1t} + u_{1x} - \frac{\beta^2}{3}\eta_{1xxt} = F_1(\eta_0, u_0, v_0, G; x, X, y, t), \end{aligned} \tag{27}$$

from (16), where $G(X, y, T) = \frac{\varepsilon f(X,y,T)}{\alpha}$ and

$$F_1 = -v_{0y} + \frac{\beta^2 \eta_{0yyt}}{3} - u_{0X} - u_0\eta_{0x} - Gu_{0x} - \eta_0 u_{0x} + \frac{2\beta^2(\eta_{0xXt} + G\eta_{0xxt})}{3}. \tag{28}$$

Cross differentiation of the momentum and continuity equations, making use of (26), and combining the results into a single equation, leads to

$$\begin{aligned} \alpha^0: \quad & \mathcal{L}\eta_0 = 0 \\ \alpha^1: \quad & \mathcal{L}\eta_1 = \mathcal{G}_1(\eta_0, u_0, v_0, G; x, X, y, t), \end{aligned} \tag{29}$$

where

$$\mathcal{L} = \partial_{tt} - \partial_{xx} - \frac{\beta^2}{3}\partial_{xxtt}. \tag{30}$$

$\mathcal{L}$ is a linear operator that shows up at every order. The inhomogeneous term $\mathcal{G}_1$ is

$$\begin{aligned} \mathcal{G}_1 = \; & (1 + \beta^2\partial_{tt}/3)\eta_{0yy} + G(1 + 2\beta^2\partial_{tt}/3)\eta_{0xx} + 2(1 + \beta^2\partial_{tt}/3)\eta_{0xX} \\ & + (u_0^2/2)_x - (u_0\eta_0)_{xt}. \end{aligned} \tag{31}$$

The order of RB and the two-scale technique restrict the region of validity of the present model. The lowest-order solutions, which are linear, are valid for distances that are less than $O(1/k\alpha)$, the scale over which triads of Fourier modes

exchange significant energy. Higher-order terms and processes neglected in the expansion restrict the range of the present nonlinear solutions to distances less than $O(1/k\alpha^2)$. Thus, RB is not formally valid for very long evolution distances. Boussinesq equations are strictly valid for $S = O(1)$, but they are quite robust [50]. In this study, the value of S is in the range of 10 to 30.

To continue, we assume that the shoreward velocity is

$$\begin{aligned} u(x,X,y,t) &= \textstyle\sum_{j=1}^{\infty}[a_j(X,y)+O(\alpha)]e^{i(k_jx-\omega_jt)}+c.c. \\ &\quad +\textstyle\sum_{j=1}^{\infty}[b_j(X,y)+O(\alpha)]e^{i(-k_jx-\omega_jt)}+c.c., \end{aligned} \tag{32}$$

where c.c. stands for complex conjugate of the expression immediately preceding its appearance. The a's are the complex incident wave amplitudes, and the b's are the complex reflected wave amplitudes. The reality of the physical variables implies that $a_{-j} = a_j^*$ and $b_{-j} = b_j^*$. The spanise velocity at the surface must then be

$$\begin{aligned} v(x,X,y,t) &= \textstyle\sum_{j=1}^{\infty}-\frac{i}{k_j}[a_{jy}(X,y)+O(\alpha)]e^{i(k_jx-\omega_jt)}+c.c. \\ &\quad +\textstyle\sum_{j=1}^{\infty}-\frac{i}{k_j}[b_j(X,y)+O(\alpha)]e^{i(-k_jx-\omega_jt)}+c.c. \end{aligned} \tag{33}$$

in order to satisfy Equation (18). Since, to lowest order, $u_{0t}+\eta_{0x} = 0$, an expression for the surface amplitude is readily available: the replacement of the lowest-order velocity into the momentum equation yields

$$\begin{aligned} \eta_0 &= \sum_{j=1}^{\infty}\frac{\omega_j}{k_j}[a_j(X,y)+O(\alpha)]e^{i(k_jx-\omega_jt)}+c.c. \\ &\quad +\sum_{j=1}^{\infty}\frac{\omega_j}{k_j}[b_j(X,y)+O(\alpha)]e^{i(-k_jx-\omega_jt)}+c.c. \end{aligned} \tag{34}$$

A solution of the form given by Equations (32), (33), and (34) is valid provided that the following relation holds between the frequency and the wavenumber:

$$\omega_j^2 - \frac{k_j^2}{1 + \beta^2 \frac{k_j^2}{3}} = 0, \tag{35}$$

which gives the dispersion relation for the j-th mode, the positive root k_j corresponding to the shoreward-directed wave, and the negative to the seaward wave.

The solution must also satisfy a compatibility condition. Since the linear operator $\mathcal{L}$ in Equation (29) appears in every order, and terms of lower-order appear in the inhomogeneous part, secular terms arise. It is an artifice of having truncated the expansion and is typified by the possibility of blowup from resonance. This resonance condition for j-th interacting waves is

$$\begin{aligned} k_j \pm \cdots \pm k_2 \pm k_1 &= 0 \\ \omega_j + \cdots + \omega_2 + \omega_1 &= 0. \end{aligned} \tag{36}$$

where the wavenumbers and corresponding frequencies obey the dispersion relation. In the scaling adopted in this study, the $O(k_j) = O(\omega_j)$.

Since the dispersion relation for gravity water waves is such that $\omega'(\kappa) > 0$ and $\omega''(\kappa) < 0$, perfect coincidence is not possible. At most we expect what we refer to as "slight resonance." Furthermore, we shall restrict our attention to the special weakly resonant triad case in which $k_2 = 2k_1 - \delta$, $\omega_2 = 2\omega_1$, where the detuning parameter $\delta \leq 0$. The compatibility condition is

$$\frac{jk_1}{2\pi} \int_{X_0}^{X_0 + 2\pi/jk_1} e^{\pm ijk_1 x} (\mathcal{G}_j + \mathcal{G}_j^*) dx = 0, \text{where } j = 1, 2, 3..., \tag{37}$$

starred quantities conjugated.

Application of the compatibility condition to the lowest-order terms in Equation (31) yields, after some algebra, the evolution equations for the modes in Equation (32), and Equation (34):

$$\begin{aligned} a_{1x} + i\varepsilon f D_1 E_1 a_1 - i\alpha F_1 a_{1yy} + i\alpha D_1 S_1 e^{-i\delta_x} a_1^* a_2 &= 0 \\ a_{2x} + i\varepsilon f D_2 E_2 a_2 - i\alpha F_2 a_{2yy} + i\alpha D_2 S_2 e^{+i\delta_x} a_1^2 &= 0 \\ b_{1x} - i\varepsilon f D_1 E_1 b_1 + i\alpha F_1 b_{1yy} - i\alpha D_1 S_1 e^{+i\delta_x} b_1^* b_2 &= 0 \\ b_{2x} - i\varepsilon f D_2 E_2 b_2 + i\alpha F_2 b_{2yy} - i\alpha D_2 S_2 e^{-i\delta_x} b_1^2 &= 0, \end{aligned} \tag{38}$$

having substituted back $X = ax$. The constants are

$$\begin{aligned} D_j &= [2(1 - \beta^2 \tfrac{\omega_j^2}{3})]^{-1} \\ E_j &= k_j(1 - \tfrac{2}{3}\beta^2\omega_j^2) \\ F_j &= 1/2k_j \\ S_1 &= \tfrac{k_2 - k_1}{\omega_1}\{k_2 - k_1 + \omega_1(\tfrac{\omega_1}{k_1} + \tfrac{\omega_2}{k_2})\} \\ S_2 &= 2(k_1^2/ + 2\omega_1^2)/\omega_2. \end{aligned} \tag{39}$$

Equation (38), along with appropriate boundary conditions, determines in an approximate way the ocean surface. The incident and reflected waves are decoupled owing to the assumptions and restrictions on the spatial variation of the bottom topography. If the spatial scales of variation in the bottom topography in the shoreward direction are of the same order as those of the surface waves, then scattering plays an important role in the energetics of these surface waves; hence the reflected component must be included even if the backwash is negligible. If, on

the other hand, the longshore sand ridges being considered were

$$h(x, X, y, T) = 1 + \varepsilon f(x, X, y, T), \tag{40}$$

the resulting modal equations, to lowest order, would be

$$\begin{aligned}
a_{1x} - i\varepsilon f D_1 E_1 \gamma_1 a_1 + i\varepsilon f D_1 E_1 \mu_1^- b_1 - i\alpha F_1 a_{1yy} + i\alpha D_1 S_1 e^{-i\delta x} a_1^* a_2 &= 0 \\
a_{2x} - i\varepsilon f D_2 E_2 \gamma_2 a_2 + i\varepsilon f D_2 E_2 \mu_2^- b_2 e^{2i\delta x} - i\alpha F_2 a_{2yy} + i\alpha D_2 S_2 e^{+i\delta x} a_1^2 &= 0 \\
b_{1x} + i\varepsilon f D_1 E_1 \gamma_1 b_1 - i\varepsilon f D_1 E_1 \mu_1^+ a_1 + i\alpha F_1 b_{1yy} - i\alpha D_1 S_1 e^{+i\delta x} b_1^* b_2 &= 0 \\
b_{2x} + i\varepsilon f D_2 E_2 b_2 - i\varepsilon f D_2 E_2 e^{-i2\delta x} \mu_2^+ a_2 + i\alpha F_2 b_{2yy} - i\alpha D_2 S_2 e^{-i\delta x} b_1^2 &= 0,
\end{aligned} \tag{41}$$

to $O(\delta/X)$, with

$$\begin{aligned}
\gamma_j &= \frac{jk_1}{2\pi} \int_0^{2\pi/jk_1} (f_{xx} + 2ik_j f_x - k_j^2 f) dx \\
\mu_j^- &= \frac{jk_1}{2\pi} \int_0^{2\pi/jk_1} (f_{xx} + 2ik_j f_x - k_j^2 f) e^{-2ijk_1 x} dx \\
\mu_j^+ &= \frac{jk_1}{2\pi} \int_0^{2\pi/jk_1} (f_{xx} + 2ik_j f_x - k_j^2 f) e^{+2ijk_1 x} dx.
\end{aligned} \tag{42}$$

The most striking differences between the way Equations (38) and (41) describe the surface is that, in the latter case, the terms involving the bottom topography, which attenuate and modulate the waves as they propagate, involve the bottom topography, its slope, and its curvature; and the energy in the reflected wave does not depend exclusively on the boundary conditions.

3 The Mass Transport Problem

The drift velocity is the second-order steady state flow that is created by the passage of overlying water waves in the sediment-laden boundary layer that hugs the bottom topography. The boundary layer is assumed to have a characteristic thickness $\delta_{bl} \ll h_0$. The sediment in the boundary layer is assumed to move from place to place at a rate equal to the drift velocity. To compute the drift velocity, we must find the fluid velocity immediately outside of the sediment-laden boundary layer. ¿From Equation (5) in scaled variables, the shoreward velocity is explicitly

$$\begin{aligned} U_b &\equiv \hat{x}\cdot\mathbf{U}(\mathbf{r},-h,t) \\ &= u(\mathbf{r},t) - \beta^2\{-h[(hu_{xx}(\mathbf{r},t)) + \alpha(hv_{xy}(\mathbf{r},t))] + \tfrac{1}{2}h^2(u_{xx}(\mathbf{r},t) + \alpha v_{xy}(\mathbf{r},t))\}, \end{aligned} \tag{43}$$

and the spanwise velocity

$$\begin{aligned} V_b &\equiv \hat{y}\cdot\mathbf{U}(\mathbf{r},-h,t) \\ &= v(\mathbf{r},t) - \beta^2\{-h[(hu_{xy}(\mathbf{r},t)) + \alpha(hv_{yy}(\mathbf{r},t))] + \tfrac{1}{2}h^2(u_{xy}(\mathbf{r},t) + \alpha v_{yy}(\mathbf{r},t))\} \end{aligned} \tag{44}$$

in the neighborhood of the boundary layer. If we neglect the reflected component, the bottom velocities to lowest order are

$$\begin{aligned} U_{0b} &= u_0 + \beta^2\tfrac{h^2}{2}u_{0xx} \\ &= \textstyle\sum_{j=1}^{2} C_j a_j(X,y)e^{i(k_j x-\omega_j t)} + c.c. \\ V_{0b} &= v_0 + \beta^2\tfrac{(h^2)_y}{2}u_{0x} + \beta^2\tfrac{h^2}{2}u_{0xy} \\ &= -i\textstyle\sum_{j=1}^{2}\tfrac{1}{k_j}[C_j a_{jy}(X,y) + i\beta^2\tfrac{k_j}{2}(h^2)_y]e^{i(k_j x-\omega_j t)} + c.c., \end{aligned} \tag{45}$$

where $C_j = 1 - \beta^2 k_j^2 \frac{h^2}{2}$.

3.1 Hydrodynamics of the Boundary Layer

In the boundary layer the transverse momentum, vertical momentum, and the continuity equations are, respectively,

$$\begin{aligned} \mathbf{u}_t + \mathbf{u}\cdot\nabla\mathbf{u} + \bar{w}\mathbf{u}_z &= -\tfrac{1}{\rho}\nabla p + \nu\Delta\mathbf{u} + \nu\mathbf{u}_{zz} \\ \bar{w}_t + \mathbf{u}\cdot\nabla\bar{w} + \bar{w}\bar{w}_z &= -\tfrac{1}{\rho}p_z + g + \nu\Delta\bar{w} + \nu\bar{w}_{zz} \\ \nabla\cdot\mathbf{u} + \bar{w}_z &= 0, \end{aligned} \tag{46}$$

where ν is the assumed isotropic eddy viscosity. Across the boundary layer the flow velocity changes from zero at the bottom boundary to some finite value characteristic of the exterior inviscid fluid. The derivatives with respect to z of any flow quantity are thus, in general, much greater than those with respect to x or y. Hence, within the boundary layer, $|\nabla\mathbf{u}| \ll |u_z|$, $|\nabla^2\mathbf{u}| \ll |u_{zz}|$, etc. We conclude that the transverse momentum in Equation (46) is well approximated by

$$\mathbf{u}_t + \mathbf{u}\cdot\nabla\mathbf{u} + \bar{w}\mathbf{u}_z = -\frac{1}{\rho}\nabla p + \nu\mathbf{u}_{zz}. \tag{47}$$

The velocity $\bar{w}$ must also be small. The continuity statement in Equation (46) suggests that the boundary layer and $\bar{w}$ are of equal order of smallness. Therefore, none of the terms on the left-hand side of Equation (47) can be neglected. On the other side of the equation, it is expected that $\nu\mathbf{u}_{zz}$ be of comparable size to the inertial terms. The magnitude of the inertial terms is represented by the size of $\mathbf{u}\cdot\nabla\mathbf{u}$; hence, the balance is such that $O(\mathbf{u}\cdot\nabla\mathbf{u}/\nu\mathbf{u}_{zz}) = 1$ when the

Reynolds number is sufficiently large, so it is mostly true in the whole boundary layer. If $\sqrt{gh_0}$ is representative of the magnitude of the velocity $\mathbf{u}$ and λ represents a distance in the transverse direction over which $\mathbf{u}$ changes appreciably, then $(\sqrt{gh_0})^2/\lambda = O(\mathbf{u}\cdot\nabla\mathbf{u})$. Since δ_{bl} is the boundary layer thickness, $\nu\sqrt{gh_0}/\delta_{bl}^2$ is a measure of $\nu\mathbf{u}_{zz}$. Thus,

$$O(\delta_{bl}^2 R/\lambda^2) = 1, \text{ where } R = \frac{\sqrt{gh_0}\lambda}{\nu}. \tag{48}$$

The dimensionless constant R is the Reynolds number. Equation (48) implies that $\delta_{bl} \sim \lambda R^{-1/2}$ as $R \to \infty$, which suggests that the boundary layer concept improves as $R \to \infty$ and that $\delta_{bl} \propto \lambda^{1/2}\nu^{1/2}$. In this study λ is large but of finite length. We assume that the boundary layer does not change significantly as a function of wave frequency. Thus, λ can be replaced by h_0 in R, so that $R = \sqrt{gh_0}h_0/\nu$. We arrive, then, at a working definition for the boundary layer thickness:

$$\delta_{bl} = \sqrt{\nu/h_0(gh_0)^{1/2}}, \tag{49}$$

which is nondimensionalized by dividing by h_0. In this scaling, it is implied that the size of the Reynolds number and the boundary layer thickness are controlled mostly by the viscous effects (i.e., the size of ν).

To get an estimate of the size of $\bar{w}$, we conclude from the continuity condition in Equation (46) that

$$O(\bar{w}_z/\nabla\mathbf{u}) = \delta_{bl}h_0/\lambda = \beta\sqrt{gh_0}R^{-1/2}; \tag{50}$$

thus

$$\bar{w} = O(\beta\sqrt{gh_0}R^{-1/2}). \tag{51}$$

With Equation (51) in hand, we can infer from the vertical momentum balance that

$$g + \frac{p_z}{\rho} = O(\delta_{bl}). \tag{52}$$

Hence $p_z = O(\delta_{bl})$; that is, the pressure is approximately constant throughout the layer.

For high Reynolds number flow, with $\delta_{bl}n = z + h$, where $\bar{z} = R^{1/2}z$ and $w = R^{1/2}\bar{w}$, the equations for the boundary layer are

$$\begin{aligned}
\beta u_t + \alpha\beta[uu_x + \alpha v u_y] + \alpha w u_n &= -\frac{\beta}{\alpha}p_x + u_{nn} \\
\beta v_t + \alpha\beta[uv_x + \alpha v v_y] + \alpha w v_n &= -\frac{\beta}{\alpha}p_y + v_{nn} \\
p_n &= O(\delta_{bl}) \\
\beta(u_x + \alpha v_y) + w_n &= 0,
\end{aligned} \tag{53}$$

having invoked the scaling that reflects weak y dependence of the flow as well. A locally flat bed has been assumed. In contrast, suppose that the bed had some finite curvature K, say. This would change the vertical momentum balance in Equation (53) to

$$p_n = KO(\mathbf{u}^2), \tag{54}$$

but the pressure change across the layer is still of $O(\delta_{bl})$, so we are justified in the assumption that the bed be locally flat.

The following boundary data is used to solve Equation (53):

$$u = v = w = 0 \qquad \text{at } n = 0 \tag{55}$$

and

$$\begin{aligned} u &\to U_b \\ v &\to V_b, \qquad n \to \infty. \end{aligned} \tag{56}$$

The velocity (U_b, V_b) immediately outside of the layer gives rise to the following pressure gradients:

$$\begin{aligned} -\frac{\beta}{\alpha} p_x &= \beta U_{bt} + \alpha\beta(U_b U_{bx} + \alpha V_b U_{by}) \\ -\frac{\beta}{\alpha} p_y &= \beta V_{bt} + \alpha\beta(U_b V_{bx} + \alpha V_b V_{by}). \end{aligned} \tag{57}$$

We thus have all the required information to solve for the velocities in the boundary layer. Performing the usual expansion

$$\begin{aligned} u &= \tilde{u}_0 + \alpha\tilde{u}_1 \cdots \\ v &= \tilde{v}_0 + \alpha\tilde{v}_1 \cdots, \end{aligned} \tag{58}$$

we obtain as the lowest-order equations

$$\begin{aligned} \beta\tilde{u}_{0t} - \tilde{u}_{0nn} &= \beta U_{0bt} \\ \beta\tilde{v}_{0t} - \tilde{v}_{0nn} &= \beta V_{0bt} \\ p_{0n} &= 0 \\ \beta\tilde{u}_{0x} + \tilde{w}_{0n} &= 0. \end{aligned} \tag{59}$$

A solution of Equation (59) of the form

$$\tilde{u}_l = \sum_{j=1}^{2} \alpha^l P_l(x, y, n) e^{i(k_j x - \omega_j t)} + c.c., \tag{60}$$

subject to the boundary conditions given by Equations(55) and (56), is found by integrating Equation (59). The same procedure is used to obtain $\tilde{v}$. The result is

$$\begin{aligned}
\tilde{u}_0 &= \textstyle\sum_{j=1}^{2} C_j a_j (1 - e^{-n\Lambda_j}) e^{i(k_j x - \omega_j t)} + c.c. \\
\tilde{v}_0 &= i \textstyle\sum_{j=1}^{2} k_j (\beta^2 (h^2)_y a_j / 2 - C_j a_{jy} / k_j^2)(1 - e^{-n\Lambda_j}) e^{i(k_j x - \omega_j t)} + c.c. \\
\tilde{w}_0 &= i\beta \textstyle\sum_{j=1}^{2} k_j C_j a_j (1 - n\Lambda_j - e^{-n\Lambda_j}) / \Lambda_j e^{i(k_j x - \omega_j t)} + c.c.,
\end{aligned} \tag{61}$$

where $\Lambda_j = (1 - i)\sqrt{\beta\omega_j / 2}$. The vertical velocity $\tilde{w}$ is found by integrating the continuity equation.

3.2 The Drift Velocity

In this section we follow closely Longuett-Higgins's study on mass transport by oscillatory flows [21]. Define the time average of the quantity A as

$$\langle A \rangle \equiv \frac{\omega}{2\pi} \int_t^{t + \frac{2\pi}{\omega}} A(s) ds = \frac{1}{\tau} \int_t^{t+\tau} A(s) ds. \tag{62}$$

The drift velocity is the time average displacement rate of a fluid particle.

As Stokes noted [22], the drift velocity is second order in nature. That is, if $\tilde{u}(\mathbf{r}, z, t)$ is the Eulerian velocity, and the motion is periodic,

$$\tilde{u}(\mathbf{r}, z, t + \tau) = \tilde{u}(\mathbf{r}, z, t), \tag{63}$$

and expressible as the asymptotic series

$$\tilde{u} = \tilde{u}_0 + \alpha^1 \tilde{u}_1 + \alpha^2 \tilde{u}_2 + \cdots, \tag{64}$$

then $\langle \tilde{u}_0 \rangle = 0$ is a statement of this assumption; in other words, the lowest-order steady-state current is zero. Let $\mathbf{U}(\mathbf{r}_0, z_0, t_0)$ denote the Lagrangian velocity, or velocity of a fluid particle at $t = t_0$ with position $(\mathbf{r}_0, z_0)$. Then, the displacement of the particle from its original position to some other position

$$(\mathbf{r}, z) = (\mathbf{r}_0, z_0) + \int_{t_0}^{t} \mathbf{U}(\mathbf{r}_0, z_0, \tilde{t}) d\tilde{t} \tag{65}$$

at time t. It follows that

$$\mathbf{U}(\mathbf{r}, z, t) = \tilde{u}[(\mathbf{r}_0, z_0) + \int_{t_0}^{t} \mathbf{U}(\mathbf{r}_0, z_0, \tilde{t}) d\tilde{t}, t], \tag{66}$$

which can be formally expanded in a Taylor series

$$\begin{aligned} \mathbf{U}(\mathbf{r}, z, t) \;=\; & \tilde{u}(\mathbf{r}_0, z_0, t) + \textstyle\int_{t_0}^{t} \mathbf{U} d\tilde{t} \cdot \nabla_{(\mathbf{r}_0, z_0)} \tilde{u}(\mathbf{r}_0, z_0, t) \\ & + \tfrac{1}{2} \{ \textstyle\int_{t_0}^{t} \mathbf{U} d\tilde{t} \}^T \cdot H_{(\mathbf{r}_0, z_0)} \tilde{u}(\mathbf{r}_0, z_0, t) \cdot \textstyle\int_{t_0}^{t} \mathbf{U} d\tilde{t} + \cdots . \end{aligned} \tag{67}$$

Here H stands for the Hessian, and both the Hessian and gradients have subscripts to remind us as to where they are to be evaluated. The steady-state Lagrangian velocity is in fact akin to the drift velocity. An approximate expression for it, in terms of the Eulerian velocity in the boundary layer, can be obtained by expanding

$$\mathbf{U} = \mathbf{U}_0 + \alpha^1 \mathbf{U}_1 + O(\alpha^2) \tag{68}$$

and substituting Equations (68) and (64) into Equation (67), order by order. After time-averaging, the lowest-order velocities are

$$\begin{aligned} O(\alpha^0): \quad \langle \mathbf{U}_0 \rangle &= \langle \mathbf{u}_0 \rangle = 0 \\ O(\alpha^1): \quad \langle \mathbf{U}_1 \rangle &= \langle \mathbf{u}_1 \rangle + \langle \int^t \mathbf{u}_0 d\tilde{t} \cdot \nabla \mathbf{u}_0 \rangle. \end{aligned} \tag{69}$$

The drift velocity is then

$$(\mathcal{U}, \mathcal{V}) = \alpha^1 \mathbf{U}_1 + O(\alpha^2). \tag{70}$$

Expressing the $O(\alpha)$ in component form, after weak y dependence scaling has been adopted, the drift velocity is

$$\begin{aligned} \mathcal{U} &= \langle u_1 \rangle + \langle \int^t u_0 d\tilde{t} u_{0x} \rangle + \langle \int^t w_0 d\tilde{t} u_{0n} \rangle \\ \mathcal{V} &= \langle v_1 \rangle + \langle \int^t u_0 d\tilde{t} v_{0x} \rangle + \langle \int^t w_0 d\tilde{t} v_{0n} \rangle. \end{aligned} \tag{71}$$

3.3 The Mass Transport Equation

Since the mean slopes in the regions of principal interest here are very low, downslope gravitational transport, which is important in the coastal environment, plays a negligible role in the formation of sand ridges, we assume that sediment movement in regions sufficiently removed from the shoaling region is accomplished primarily by suspension. Hence, we adopt results from the Longuett-Higgins theory to characterize the effect of the water waves on the fluid motion in the boundary layer. Furthermore, since the ratio of bar height to separation is significantly below the critical value of 0.1 (which has been identified by Sleath [12] as the value over which

flow in the boundary layer separates behind the crests of the bars and vortex formation takes place), the flow in the boundary layer is adequately characterized by the lowest-order dynamical quantities. In what follows, the fluid wave field is assumed to be entirely represented by the incident wave. Further, we assume that the viscous boundary layer is sediment-laden, composed of cohesionless, rarely interacting, sand particles.

The sediment concentration ρ in coastal environments has a very weak influence on the fluid flow [51]. Typical values for the concentration are $\rho \sim 10^{-3} - 10^{-4}$ ppm, and this situation is assumed thoughout the shelf. Chapalain [51] and Boczar-Karakiewicz et al. [52] concluded that time independent and vertically uniform parameters of eddy viscosity and eddy diffusivity are adequate in providing satisfactory accuracy for sediment morphology models on the shelf In this study we adopt a very simple model for the sediment concentration [12].

The equation of continuity for the sediment concentration is the advection-diffusion equation

$$\rho_t + \nabla\cdot(\mathbf{u}\rho) + [(w - v_f)\rho]_n = 0, \tag{72}$$

where v_f is the sediment "fall velocity" and $n = (z + h(X, y, T))/\delta_{bl}$. Assume that, apart from random fluctuations, $\mathbf{u}$ and ρ do not vary much over small transverse spatial scales, so that the second term of the above equation may be neglected. In light of this, the sediment concentration changes at a rate $\partial\rho/\partial n$ proportional to the vertical flux. Hence,

$$w\rho = -\gamma\rho_n, \tag{73}$$

where γ is the diffusivity constant.

The flux, which is the product of the concentration and the velocity, can be split into a time-dependent part C^t and a time-independent part C^m. Boczar-Karakiewicz et al. [6] found that in the sand ridge areas, the ratio $C^t/C^m = O(10^{-2})$ for the off-shore case. This situation isl assumed to apply throughout the shelf, so that the sediment concentration is represented solely by its time-independent part. Employing this assumption and substituting Equation (73) into Equation (72), we have as the equation for sediment concentration

$$\gamma\rho_n + v_f\rho = 0. \tag{74}$$

The boundary condition may be taken as

$$\frac{\gamma}{v_f}\frac{\partial\rho}{\partial n} = P(\mathbf{r}), \tag{75}$$

where $P(\mathbf{r})$ has the flavor of Svendsen's [53] empirical "pick-up function," which incorporates such effects as the degree of wave asymmetry and skewness of sediment flux, and a Shield's parameter, which sets a threshold fluid velocity at which sediment will be picked up, based on the sediment particles' buoyancy and geometry and on the fluid's velocity field and viscocity.

Solving Equation (74), we obtain as the sediment concentration

$$\rho = P(\mathbf{r})e^{-\sigma n}, \tag{76}$$

where $\sigma = v_f/\gamma$. The fall velocity v_f is species-dependent. It is either measured or estimated by calculating the balance of drag to buoyant forces for a particle

falling freely into a static fluid. The diffusivity constant γ is hard to estimate: sedimentologists usually measure its value in the field.

For the sake of clarity, the mass transport equation is derived by assuming transverse dependence in the x direction only. The generalization to variations in y follow in a straightforward manner. Let $T \in [0, \infty)$ and $\Pi_T \in \mathcal{R}^1 \times [h(T), \zeta]$, where $\zeta \geq h(T) + \delta_{bl}$, be the boundary layer time-space domain, and consider a differential "volume" element in such a domain, as shown in Figure 5, which is bounded on the bottom by the ocean topography and on the top by a flat lid $z' = \zeta$. It is assumed

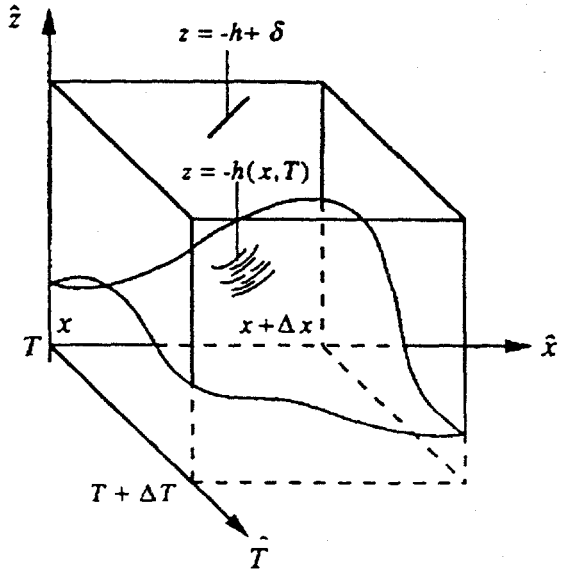

Figure 5: Volume element used in the derivation of the mass trasport equation

that the sediment concentration ρ is entirely negligible for $z' > \zeta$ and moves on fast time scales. In what follows $\rho : \Pi_T \longmapsto \mathcal{R}^1$. The sediment concentration and

drift velocity are thought to be $C^1(\Pi_T)$, and the bottom topography $h \in C^1(T)$, and piecewise linear in Π_T.

The mass flux per unit length at x in a time interval $[T, T+\Delta T]$ is given by

$$\int_T^{T+\Delta T} d\tau \int_{h(x,\tau)}^{\zeta} dz' \rho(x,z') \mathcal{U}(x,z') \equiv \int_T^{T+\Delta T} d\tau \int_{h(x,\tau)}^{\zeta} dz' M(x,z'). \qquad (77)$$

Consider a portion of the region, say $[x, x+\Delta x]$, in a time interval $[T, T+\Delta T]$. Since mass cannot spontaneously vanish or be created, the net amount of sediment between point x and $x+\Delta x$ must be compensated by a change in the concentration of the sediment or by a topographical change in the bottom surface. The flux difference in the space and time intervals $[x, x+\Delta x]$, $[T, T+\Delta T]$ is thus

$$\int_T^{T+\Delta T} d\tau \int_{h(x+\Delta x,\tau)}^{\zeta} dz' M(x+\Delta x, z') - \int_T^{T+\Delta T} d\tau \int_{h(x,\tau)}^{\zeta} dz' M(x,z'), \qquad (78)$$

and the total mass in the given portion at time T is given by

$$\int_x^{x+\Delta x} d\xi \int_{h(\xi,T)}^{\zeta} dz' \rho(\xi, z'). \qquad (79)$$

The change in total mass in a time interval $[T, T+\Delta T]$ resulting from net accumulation is given by

$$\int_x^{x+\Delta x} d\xi \int_{h(\xi,T+\Delta T)}^{\zeta} dz \rho(\xi, z') - \int_x^{x+\Delta x} d\xi \int_{h(\xi,T)}^{\zeta} dz' \rho(\xi, z'), \qquad (80)$$

or equivalently,

$$\int_x^{x+\Delta x} d\xi \int_{h(\xi,T)}^{h(\xi,T+\Delta T)} dz' \rho(\xi, z'). \qquad (81)$$

Equating (78) and (81), dividing by $\Delta x \Delta T$, and formally taking the limit as Δx and ΔT go to zero, we obtaian, on the right-hand side,

$$\begin{aligned} \lim_{\Delta T \to 0 \Delta x \to 0} \frac{1}{\Delta x \Delta T} \int_x^{x+\Delta x} d\xi \int_{h(\xi,T)}^{h(\xi,T+\Delta T)} dz' \rho(\xi, z') &\sim \\ \lim_{\Delta T \to 0 \Delta x \to 0} \frac{1}{\Delta x \Delta T} \int_x^{x+\Delta x} d\xi \int_{h(\xi,T)}^{h(\xi,T)+\Delta T \frac{\partial h(\xi,T)}{\partial T}} dz' \rho(\xi, z') &= \\ \rho(x, h(x,T)) \frac{\partial h(x,T)}{\partial T}, & \end{aligned} \tag{82}$$

and on the other side of the equation,

$$\begin{aligned} &\lim_{\Delta T \to 0 \Delta x \to 0} \frac{1}{\Delta x \Delta T} \int_T^{T+\Delta T} d\tau \{ \int_{h(x+\Delta x,\tau)}^{\zeta} dz' M(x+\Delta x, z') - \int_{h(x,\tau)}^{\zeta} dz' M(x,z') \} = \\ &\lim_{\Delta T \to 0 \Delta x \to 0} \frac{1}{\Delta x \Delta T} \int_T^{T+\Delta T} \{ \int_{h(x+\Delta x,\tau)}^{\zeta} dz' [M(x,z') + \Delta x \frac{\partial M}{\partial x}(x,z') + \cdots] - \\ &\int_{h(x,\tau)}^{\zeta} M(x,z') \} = \lim_{\Delta T \to 0 \Delta x \to 0} \frac{1}{\Delta x \Delta T} \Delta x \int_{h(x,\tau)+\Delta x \frac{\partial h}{\partial x}}^{\zeta} dz' \frac{\partial M}{\partial x}(x,z') = \\ &\int_{h(x,T)}^{\zeta} dz' \frac{\partial M}{\partial x}(x,z') \end{aligned} \tag{83}$$

Hence, the mass transport equation is

$$\frac{\partial h(x,T)}{\partial T} = \frac{K'}{\rho(x, h(x,T))} \frac{\partial}{\partial x} \int_{h(x,T)}^{\zeta} \rho(x,z') \mathcal{U}(x,z') dz', \tag{84}$$

where K' is a constant of proportionality. Since the boundary layer is assumed very thin, we may define the mass transport flux as

$$\begin{aligned} \mu &\equiv \int_0^{\delta_{bl}} \rho(x,z') \mathcal{U}(x,z')) dz' \\ \nu &\equiv \int_0^{\delta_{bl}} \rho(x,z') \mathcal{V}(x,z')) dz', \end{aligned} \tag{85}$$

so that the transport equation now reads

$$\frac{\partial h(x,T)}{\partial T} = \frac{K}{\rho_0}\mu_x. \tag{86}$$

The generalization of Equation (86) to one more space dimension is

$$\frac{\partial h(x,y,T)}{\partial T} = \frac{K}{\rho_0}(\mu_x + \nu_y), \tag{87}$$

where μ and ν are the shoreward mass flux and the longshore mass flux, respectively. Note that when weak y dependence scaling is adopted in Equation (87), the longshore mass flux is $O(\alpha)$ smaller than all other quantities in the equation.

In the remainder of this paper, we assume, for simplicity, that the sediment concentration is constant and equal to ρ_0 in the boundary layer. In terms of Equation (71), and upon use of Equation (85), the calculation of the mass flux components, to lowest order, is

$$\mu = \sum_{j=1}^{2} \frac{2k_j C_j^2 |a_j|^2}{\omega_j \sigma_j} \mathcal{I}_{1j} + \sum_{j=1}^{2} \frac{\beta k_j C_j^2 |a_j|^2}{\sigma_j^3} \mathcal{I}_{2j} + c.c., \tag{88}$$

where

$$\begin{aligned} \mathcal{I}_{1j} &= \sigma_j \delta_{bl} - \frac{\beta\sigma_j}{2} - \frac{3}{2} + \frac{1}{2}(1 - \beta\sigma_j)e^{-2\sigma_j\delta_{bl}} \\ &\quad + e^{-\sigma_j\delta_{bl}}[\cos\sigma_j\delta_{bl} - \sin\sigma_j\delta_{bl}][1 - \beta\sigma_j(\sigma_j\delta_{bl} + 1)] \end{aligned} \tag{89}$$

and

$$\begin{aligned}\mathcal{I}_{2j} &= \frac{3}{2}(1/2 - \sigma_j\delta_{bl}) + e^{-2\sigma_j\delta_{bl}}/4 \\ &\quad -e^{-\sigma_j\delta_{bl}}[1 + \delta_{bl}\sigma_j]\cos\sigma_j\delta_{bl} + 2e^{-\sigma_j\delta_{bl}}\sin\sigma_j \end{aligned} \tag{90}$$

for the shoreward mass flux, and

$$\nu = \sum_{j=1}^{2} \frac{iC_j^2 a_j^* a_{jy}}{\omega_j \sigma_j}\mathcal{J}_j + O(\beta^3) + c.c. \tag{91}$$

for the longshore directed mass flux, with

$$\begin{aligned}\mathcal{J}_j &= \sigma_j\delta_{bl} - 1 - \frac{1}{2}(1 - e^{-2\sigma_j\delta_{bl}}) + e^{-\sigma_j\delta_{bl}}(\cos\sigma_j\delta_{bl} - \sin\sigma_j\delta_{bl}) \\ &\quad +\beta\Lambda_j[\frac{1}{2}(1 + e^{-2\sigma_j\delta_{bl}}) + e^{-\Lambda_j\delta_{bl}}(i\delta_{bl}\sigma_j/2 - 1)]. \end{aligned} \tag{92}$$

Before proceeding, two important remarks are in order. First, we note that the bottom need not be slightly perturbed to initiate the development of bars. Second, the time-scale discrepancy may be estimated by examining the ratio of the magnitude of the time rate of change of the bottom to the Eulerian velocity. Such comparison leads in a straightforward manner to the conclusion that $t/T = O(\alpha)O(\delta_{bl})O(\rho) \sim O(10^{-7})$, assuming that the boundary layer thickness is typically $O(10^{-2}h_0)$ and the sediment concentration is $O(10^{-4})$ ppm.

4 Qualitative Features of the Solutions to the Full Model

Some of the qualitative features of the full model are presented in this section, using examples computed numerically with the fixed-point

method, which is described in [54]. The main points of the section are to(1) present the effects of different initial bottom configurations and boundary conditions on the surface and on the eventual bottom topography after the passage of many surface waves, and (2) show that the smaller reflected wave plays a relatively minor role in determining the shape of the ocean surface and therefore of the sand-ridge topography when the bottom is assumed to be very mildly sloped.

To better discern the effects of different bottom topographies on the surface waves and on the eventual bottom topography after the passage of many waves, we now turn to the case in which the initial bottom configurations are strictly x-dependent and the boundary conditions are constant. Briefly, in this case, a larger number of bars form when the gradient is slight, the distance separating the bars increases seaward for the positively sloped case, and initial bottom discontinuities in the x direction tend to get "smoothed out" after the passage of many waves.

Waves at $T = 0$ that are traveling normal to the shore over topography initially described by $f = 0.006x$ are displayed in Figure 6. Superimposed, but not drawn to scale, is the eventual bottom topography. Figure 7 shows the evolution of an initially stepped bottom at three different times. For these figures $\alpha = 0.1, \varepsilon = 0.2$, $\beta = 0.08$, and $\omega_1 = 1.8$.

A bottom, which initially had gradients in the y direction, bends the water

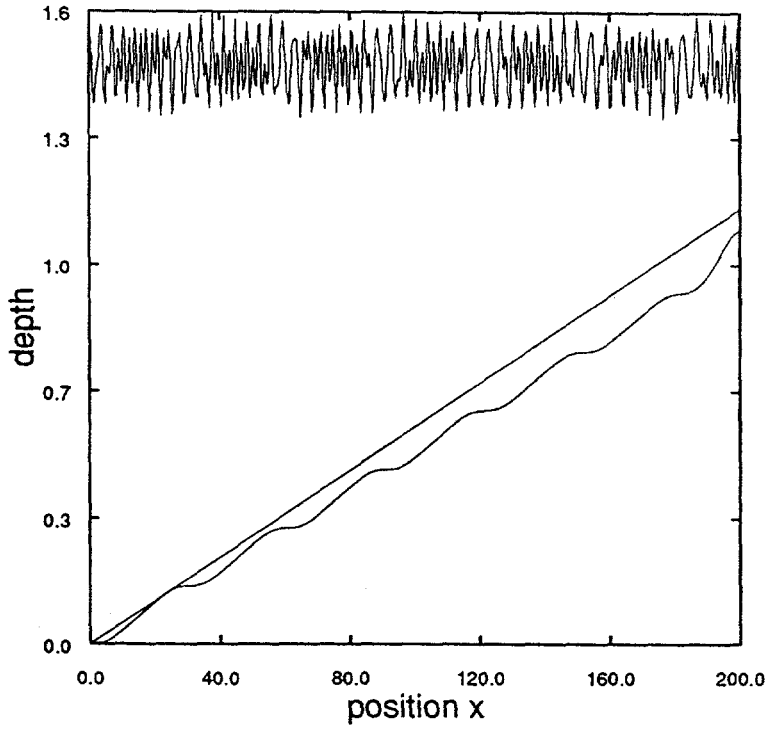

Figure 6: Ocean surface at $T = 0$. Bottom at $T = 400$, for $f(x, y, T = 0) = 0.006x$. $a_1(x = 0) = 0.5$, $a_2(x = 0) = 0.01$.

waves, affecting the eventual bottom topography by producing a series of bars with refractive features. Consider, for example, the case in which the initial bottom topography is $f(x, y) = 0.0075x - 0.005y$, with all other parameters as before, except $\omega_1 = 1.2$. Figure 8 shows a_2 at $T = 0$. A striking way in which refraction takes place can be seen in the case for which the boundary conditions at $x = 0$ are y dependent. The case for which $f(x, y) = 0$ at $T = 0$ and the boundary conditions are $\mathcal{A}_1 = 0.5+0.001y$ and $\mathcal{A}_2 = 0.02+0.001y$, corresponding to an incoming gravity wave that has slightly higher amplitude at one end than at the other, is shown in Figures 9 and 10 for $a_2(T = 0)$ and $f(T = 400\Delta T)$, respectively. The eventual fate

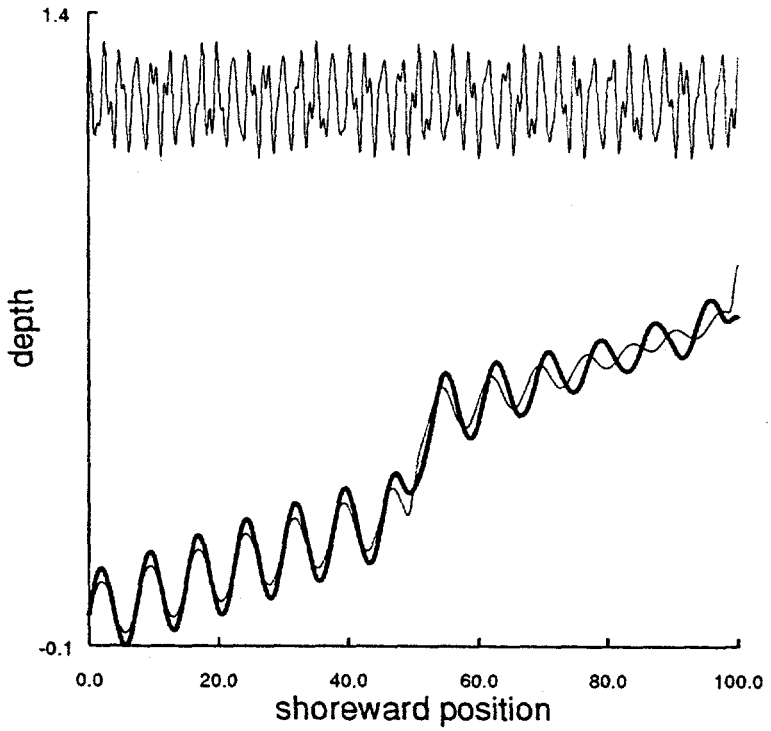

Figure 7: The fate of the topography which initially contained a step, shown at three different times

of a bottom that initially was smooth but sloped, $f(x,y) = 0.0075x - 0.005y$, is illustrated in Figures 11, 12, and 13. Compare these with Figure 8. The boundary conditions are $\mathcal{A}_1 = 0.5$ and $\mathcal{A}_2 = 0.02$.

Shown in Figure 14 is the cross section of mode $a_1(x,y)$, and in Figure 15 a comparison of the eventual bottom with and without contributions from the reflected field. Both figures were computed by using Equation (38), with $\mathcal{A}_1 = 0.5$, $\mathcal{A}_2 = 0.01$, $\mathcal{B}_1 = 0.2$, and $\mathcal{B}_2 = 0.$; $\varepsilon = 0.2$, $\alpha = 0.1$, $\beta = 0.08$. The bottom was $f(x,y) = 0.006x$ at $T = 0$. The domain was 200 units long.

As was discussed in Section 2, the reflected and incident fields are completely

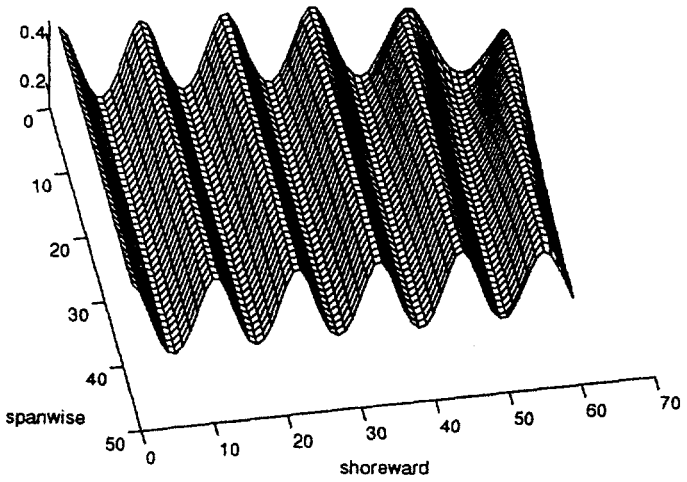

Figure 8: Refraction on the surface mode a_1 due to the bottom topography: $f(x,y) = -0.005y$ Shown at $T = 0$.

decoupled, owing to the assumptions made concerning the bottom topography. The deformations on the bottom topography due to the reflected component are entirely determined by the amount of energy in the boundary conditions. Hence, it is necessary to include the reflected component when the sea-going wave backwash is not negligible.

5 Conclusions

This study detailed the construction of a model for the formation and evolution of three-dimensional sedimentary structures on the continental shelf, based on the energetic interactions of weakly nonlinear long waves with the shelf's sedimentary topography.

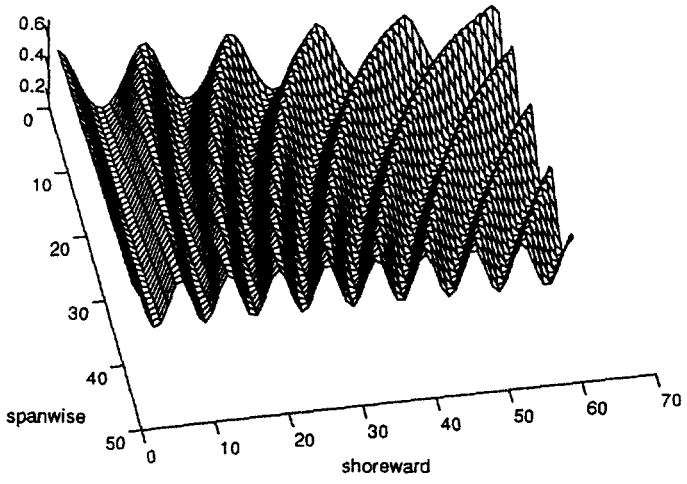

Figure 9: Refraction due to boundary conditions. a_1 at $T = 0$.

The main conjecture of this study is that a significant, but by no means exclusive, agent for the formation and evolution of longshore sand ridges on regions of the continental shelf that are sufficiently removed from the shoaling area is the repeated action of the second-order oscillatory drift velocity that results from the passage of weakly nonlinear shallow-water internal or surficial waves. The basis for the conjecture rests on (1) the close correlation between the interbar spacing and the length in which energetic exchanges among the most powerful modes of the shallow water waves takes place; (2) the close correlation between the evolutionary time scales for the bars and the time required for highly coherent nonlinear dispersive wave trains to impart sufficient energy into a boundary layer to significantly transform a sediment-laden bottom topography; (3) the fact that longshore sand ridges are found in areas in which no wave breaking occurs and/or in which the reflected field is absent or negligible; (4) the claim that sand ridges with highly

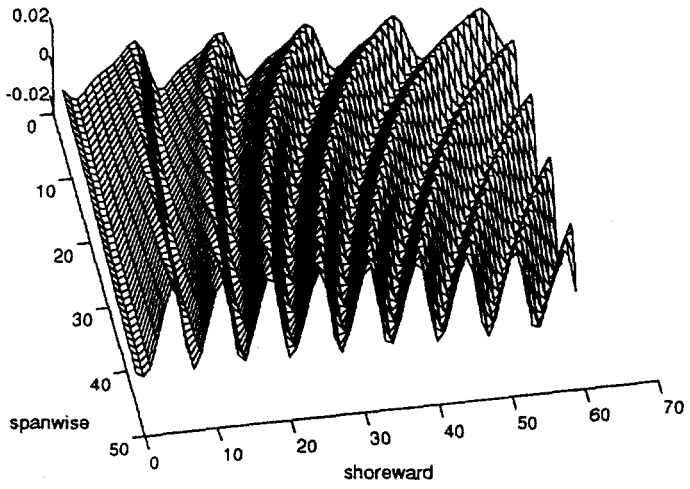

Figure 10: Refraction due to boundary conditions. Bottom at $T = 100\Delta T$.

organized characteristics may be found in regions in which coherent weakly nonlinear dispersive waves exist; and (5) the fact that the energy of these waves is of the correct magnitude to significantly affect the topography of a sediment-laden bottom.

At present, neither the dynamics of sedimentation nor those of water waves are fully understood. The model presented here represents the conjecture based on current understanding of both processes. If the conjecture is correct, the model will improve in predictive power as understanding of sedimentation and wave dynamics improve. The more important functions played by the model, however, are that its development yields clues to ways in which the conjecture itself may be refined and tested, as well as generating problems that are interesting independent of the sedimentation problem at hand, such as the modal surface system that appears in this study.

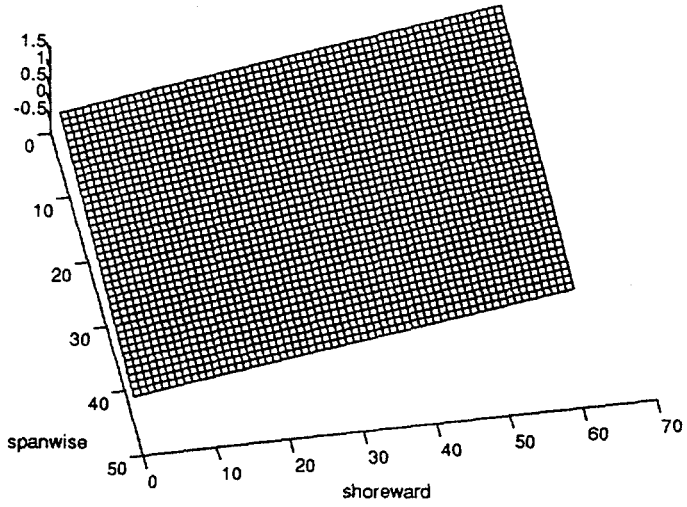

Figure 11: Evolution of bottom topography. T=0.

The model in its inception was two dimensional. Based on encouraging comparisons with actual field data, the three-dimensional version was developed. Briefly described, the present model couples a mass transport equation, which controls the history of the bottom topography, to a mathematical equation, which describes the evolution of the most energetic modes of surface weakly nonlinear dispersive shallow-water waves with weak spanwise spatial dependence. To solve the coupled system, one relies on the discrepant time scales of the bottom evolution and of the water waves to effectively decouple their interaction, making a solution by iteration possible.

In the near future the modal representation of the water waves will be replaced with a full Boussinesq system, and the effects of oceanic currents will be included in the model. Bona and Saut [55] are studying the different versions of the Boussinesq system in order to determine, among other things, which variant

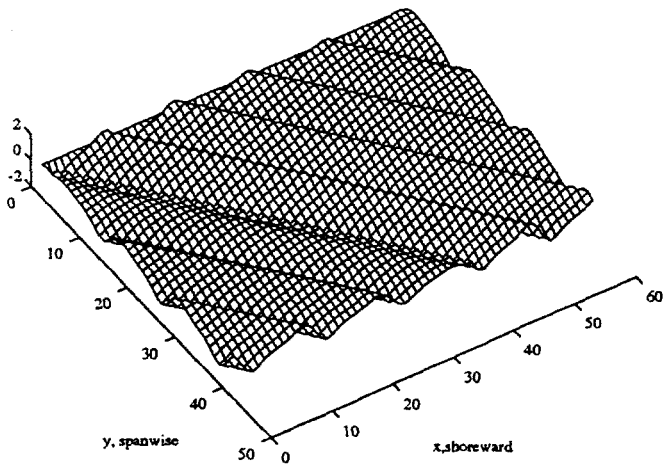

Figure 12: Evolution of bottom topography at $T = 40\Delta T$. Shown here is the difference between the new bottom and the original topography.

best models oceanic waves and which is well-posed as a boundary value problem. Additionally, a number of issues brought up in this study need to be pursued to completion. These include the search for stable bottom configurations as predicted by the model, completion of the well-posedness theory and the Hamiltonian structure for the surface system, and development of a stability result for the iterative procedure that was used to solve the coupled surface/mass transport equations.

The sensible way to test the conjecture and the model is, of course, to examine oceanic field data. Comparisons with oceanic field data can give an idea of the predictive powers of the model; laboratory experiments cannot, however, as they do not scale well. The task of making field observations, particularly in the three-dimensional case, is a tedious, expensive, and difficult enterprise. While researchers at the INRS at the University of Quebec, headed by Prof. Boczar-Karakiewicz,

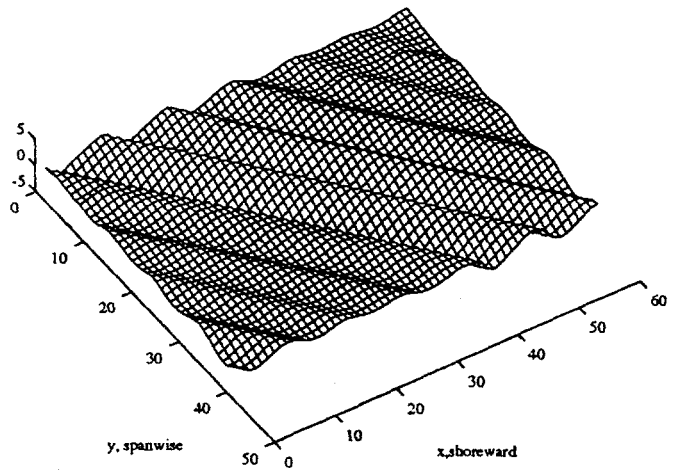

Figure 13: Evolution of bottom topography.$T = 100\Delta T$. Shown here is the difference between the new bottom and the original topography.

were able to make some comparisons between the two-dimensional version of the model and sand ridge data [41], finding that the model's predictions agreed qualitatively with the height, spacing, and evolution trends of the actual bars, they have not yet taken on the task of making comparisons in the three-dimensional case. As of this writing, the Quebec team is reducing field data from the continental shelf, gathered from the ocean floor neighboring Newfoundland and Eastern Australia in order that comparisons may be made between the three-dimensional model and data.

Several aspects of the conjecture can be tested in the laboratory. The drift velocity created by shallow water waves of the type identified here as responsible for the formation of longshore sand ridges could be observed and studied in a laboratory setting since they may be studied in a plume with a fixed bottom.

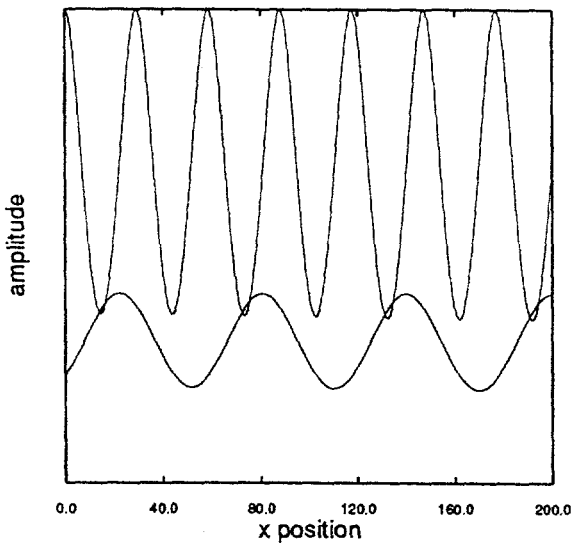

Figure 14: Profile of a_1 and b_1, for $f(x,y) = 0.006x$. $\mathcal{A}_1 = 0.5$, $\mathcal{B}_1 = 0.2$.

Comparisons between the laboratory experiments and the drift velocity measurements in sand ridge fields could prove fruitful. In particular, the model assumes that the adjustment of the bottom/surface is a gradual process; thus, it would be interesting to see whether the drift velocity is capable of changes in character to that produced by the surface waves.

Field observations are needed to (1) determine the importance of both the reflected wave field and oceanic currents in determining the nature of the drift velocity in sand ridge areas; (2) correlate in some way the beginning and end of ridge fields and the physical location at which water waves are created and eventually destroyed; (3) track the relevant wave spectra in order to see evidence of the predicted pattern in energetic interaction lengths and its correlation to features of the bottom topography; and (4) determine what sort of sand ridge configurations are stable and/or nonmigratory.

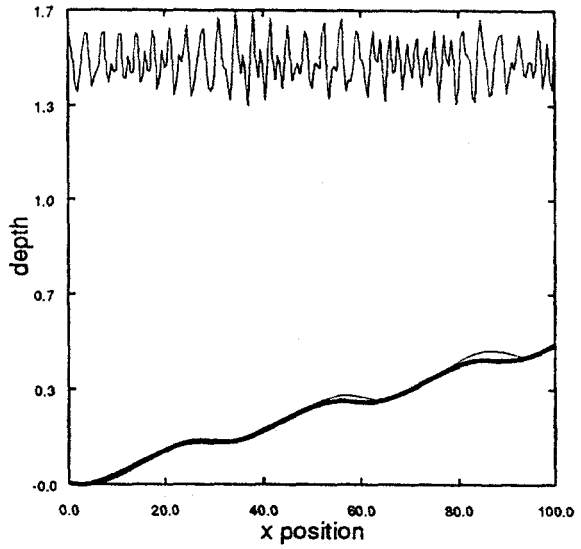

Figure 15: Effect of a bi-directional surface wave field on the eventual bottom configuration. Initially, $f(x, y, 0) = 0.006x$. The dark line is the bottom resulting from a strictly shoreward-directed wave.

Laboratory observations are required to determine how well the various Boussinesq systems model the weakly nonlinear shallow-water waves and to confirm the existence of recurrence-like solutions over long propagation lengths. Additionally, more experiments aimed at furthering our understanding of the motion of sediment in the boundary layer are needed.

Elgar and his collaborators [50] have examined the issue of the recurrence of solutions to the modally truncated Boussinesq equation numerically in the Stokes parameter regime of $O(1)$. They found that the two-mode case, which is used in this study, displays recurrence-like solutions over a great many wavelengths. They found that as the number of modes is increased, the recurrence is confined to fewer and fewer cycles; initially very narrow spectra undergo more recurrence-like

cycles, before the spectra flatten, than do initially broad-banded spectra. Their conclusion is that recurrence-like solutions are an artifice of a severely truncated modal expansion of the Boussinesq equation. If these findings prove correct (we are addressing this issue in a separate study), we may be modeling the water waves in this study incorrectly. The observations of Elgar et al. do not, however, weaken in any way our conjecture that weakly nonlinear shallow-water waves may be responsible for the formation and evolution of sand ridges, since there is more than ample observational evidence that these nonlinear waves travel over very vast spans of ocean (i.e., that their spectra recurs a great many times before they lose their coherent shape) over regions where sand ridges are a prominent feature of the ocean floor. The appropriateness of making use of a small number of modes comes from field data. Figure 16 suggests that most of the energy in the waves is found in the first few harmonics [56]. The figure also shows the shifting of energy from lower frequencies to higher ones as the wave travels shoreward over a decreasing water column depth.

Computational experiments are being planned, aimed at exploring the nature of recurrence-like solutions in nonlinear dispersive equations, such as the Boussinesq equation: other experiments will explore the stability and interdependence of the truncated modal solutions to these equations.

While comparisons between field data and the two-dimensional model are very encouraging and this three-dimensional extention should therefore find applicability in the real-world environment, any topographical chart of the continental shelf provides a good reminder of the long path yet to travel toward a complete understanding and model of the full problem. If this study has piqued the curiosity and

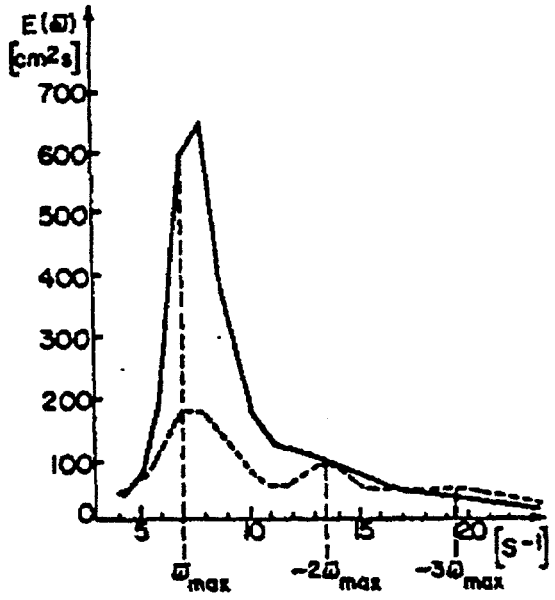

Figure 16: Energy for shallow water waves in the Southern Baltic Sea: $h_0 = 6.0m$ ————, $h_0 = 2.0m$ – – – – – – – – –. From Druet *et al.* [56].

compelled the reader to take a closer look at sandbars, it will have succeeded.

Acknowledgments

We thank the Applied Research Laboratory at The Pennsylvania State University for making this project possible. This work was also supported by the Office of Scientific Computing, U.S. Department of Energy, under Contract W-31-109-Eng-38.

List of Figures

References

[1] R. A. Davis, W. T. Fox, M. O. Hayes & J. C. Boothroyd, "Comparison of Ridge and Runnel Systems in Tidal and Non-Tidal Environments," in *Proceedings, 8th. Conference of Great Lakes Research*, Int. Ass. Great Lakes Research, 1965, 223–231.

[2] T. Off, "Rhythmic Sand Bodies Caused by Tidal Currents," *Bulletin of the American Association of Petroleum Geologists* 47 (1960), 324–341.

[3] J. R. L. Allen, in *Current Ripples*, North Holland, 1968, 434.

[4] D. J. P. Swift, "Quaternary Shelves and the Return to Grade," *Marine Geology* 1 (1968), 5–30.

[5] J. Lau & B. Travis, "Slowly Varying Stokes Waves and Submarine Longshore Bars," *Journal of Geophysics Research* 78 (1973), 4489–4497.

[6] B. Boczar-Karakiewicz, C. L. Amos & G. Drapeau, "The Origin and Stability of Sand Ridges on Sable Island Bank, Scotian Shelf," *Continental Shelf Research* 10 (1990), 683–701.

[7] A. Short, "Multiple Off-shore Bars and Standing Waves," *Journal of Geophysical Research* 80 (1975), 3838–3840.

[8] C. Dean, "Nearshore is Plumbed for Clues to Explain How Beach Waves Act," The New York Times, June 12, 1990.

[9] E. W. Bijker, E. Hijun & P. Vallinga, "Sand Transport by Waves," *Proceedings, 15th International Conference on Coastal Engineering* (1976).

[10] R. Hallermeier, "Oscillatory Bed-Load Transport," *Continental Shelf Research* 1 (1982), 159–190.

[11] S. Elgar, R. T. Guza & M. Freilich, "Eulerian Measurements of Horizontal Accelerations in Shoaling Gravity Waves," *Journal of Geophysical Research* 93 (1988), 9261–9269.

[12] J. F. A. Sleath, *Sea Bed Mechanics*, John Wiley and Sons, New York, 1984.

[13] R. A. Bagnold, "Motion of Waves in Shallow Water. Interaction of Waves and Sand Bottoms," *Proc. Roy. Soc. London Ser. A* 187 (1963), 1–15.

[14] J. A. Bailard & D. L. Inman, "An Energetics Model for a Plane Sloping Beach. Local Transport," *Journal of Geophysical Research* 75 (1970), 5800–5812.

[15] J. D. Smith, "The Stability of a Sand Bed Subjected to Shear Flow at Low Froude Number ," *Journal of Geophysical Research* 75 (1970), 5928–5940.

[16] J. Fredœ, "On the Development of Dunes in Erodible Channels," *Journal of Fluid Mechanics* 64 (1974), 1–16.

[17] K. J. Richards, "Formation of Ripples and Dunes on an Erodible Bed," *Journal of Fluid Mechanics* 99, 597–618.

[18] R. Dean, "Future Directions in Cross-shore Transport Modelling," Coastal Sediment Workshop '91, 1991.

[19] A. J. Raudkivi, "Study of Sediment Ripple Formation," *Proc. American Society of Civil Engineering, Hydraulics Division* 89 (1963), 15–36.

[20] P. B. Williams & P. H. Kemp, *Proceedings American Society of Civil Engineering* 97 (1971), 505.

[21] M. S. Longuett-Higgins, "Mass Transport in Water Waves," *Philosophical Transactions of the Royal Society of London* 245 (1953), 535–581.

[22] G. G. Stokes, *Philosophical Transactions of the Royal Society of London* 8 (1847), 441.

[23] B. Johns, "On the Mass Transport Induced by an Oscillatory Flow in a Turbulent Boundary Layer," *Journal of Fluid Mechanics* (70), 177–185.

[24] P. Blondeaux, "Sand Ripples under Sea Waves. Part 1. Ripple Formation," *Journal of Fluid Mechanics* 218 (1990), 1–17.

[25] G. Vittori & P. Blondeaux, "Sand Ripples under Sea Waves. Part 2. Finite-amplitude Development," *Journal of Fluid Mechanics* 218 (1990), 19–39.

[26] A. Holman & A. J. Bowen, "Bars, Bumps and Holes: Model for the Generation of Complex Beach Topography," *Journal of Geophysical Research* 87 (1982), 457–468.

[27] A. J. Bowen, "On-Offshore Sand Transport on a Beach, (Abstract)," *EOS, Transactions of the American Geophysical Union* 56 (1975), 83.

[28] B. Boczar-Karakiewicz, T. B. Benjamin & W. P. Pritchard, "Reflection of Water Waves in a Channel with Corrugated Bed," *Journal of Fluid Mechanics* 185 (1987), 229–247.

[29] W. G. Pritchard, Personal Communication, 1990.

[30] C. C. Mei & U. Ümlüata, "Harmonic Generation in Shallow Water Waves," in *Waves on Beaches*, R. E. Meyer, ed., Academic Press, San Diego, 1972.

[31] T. Hara & C. C. Mei, "Bragg Scattering of Surface Waves by Periodic Bars. Theory and Experiment," *Journal of Fluid Mechanics* 152 (1987), 221–241.

[32] C. C. Mei, T. Hara & M. Naciri, "Note on Bragg Scattering of Water Waves by Parallel Bars on the Sea Bed," *Journal of Fluid Mechanics* 187 (1990), 147–162.

[33] H. J. deVriend, "2DH Computation of Transient Sea Bed Evolution," in *20th International Conference on Coastal Engineering*, Taipei, 1986.

[34] R. C. H. Russell & J. D. C. Osorio, "An Experimental Investigation of Drift Profiles in a Closed Channel," *Proc. 6th. Conference on Coastal Engineering* (1975).

[35] E. W. Bijker, J. P. T. Kalkwijk & T. Pieters, "Mass Transport in Gravity Waves on a Sloping Bottom," *Proceedings, 14th Conference on Coastal Engineering* (1974).

[36] J. M. Huthnance, "Internal Tides and Waves Near the Continental Shelf," *Geophys. Astrophys. Fluid Dynamics* 48 (1989), 81–106.

[37] J. M. Suhaida, "Standing Waves on Beaches," *Journal of Geophysical Research* 79 (1974), 3065–3071.

[38] J. Lau & A. Barcilon, "Harmonic Generation of Shallow Water Waves over Topography," *Journal of Physical Oceanography* (1972).

[39] B. Boczar-Karakiewicz, B. Paplinska & J. Winieki, "Formation of Sandbars by Surface Waves in Shallow Water. Laboratory Experiments," *Rozprawy Hydrotechnisczne* (1981).

[40] B. Boczar-Karakiewicz, J. L. Bona & G. Cohen, *Interaction of Shallow-water waves and bottom topography*, PSU Applied Mathematics Series #AM3, Penn State University, 1986.

[41] B. Boczar-Karakiewicz, J. L. Bona & A. Pelchat, "Interaction of Shallow Water Internal Waves with the Bottom Topography," *Continental Shelf Research* 11 (1991), 234–345.

[42] V. E. Zakharov & A. B. Shabhat, "Exact Theory of Two-dimensional Self-focusing and One-dimensional Self-modulation of Waves in Nonlinear Media," *Soviet Physics, JETP* 34, 62–69.

[43] J. Miles, "On Hamilton's Principle for Surface Waves," *Journal of Fluid Dynamics* 83 (1977), 153–158.

[44] S. Bowman, "Hamiltonian Formulations and Long-Wave Models for Two-Fluid Systems," unpublished, 1986.

[45] T. B. Benjamin & P. J. Olver, "Hamiltonian Structure, Symmetries and Conservation Laws for Water Waves," *J. Fluid Mech.* 125 (1982), 137–185.

[46] Lord Rayleigh, "On Waves," *Philosophical Magazine* 5 (1876), 257–279.

[47] J. Boussinesq, "Theorie de l'intumescence liquid appelee onde solitaire ou de translation, se propagente dans un canal rectangulaire," *Compte Rendus Academie Scientifique, Paris* 72 (1871), 755–759.

[48] T. B. Benjamin, J. L. Bona & J. J. Mahony, "Model Equations for Long Waves in Nonlinear Dispersive Systems," *Philosophical Transactions of the Royal Society* A 227, 47–78.

[49] J. M. Restrepo, "A Model for the Formation and Evolution of Three-dimensional Sedimentary Structures on the Continental Shelf," Ph.D. thesis, The Pennsylvania State University, 1992.

[50] S. Elgar, M. Freilich & R. T. Guza, "Recurrence in Truncated Boussinesq Models of Nonlinear Waves in Shallow Water," *Journal of Geophysical Research* 95 (1991), 11547–11556.

[51] E. Chapalain, "Etude Hydrodynamique et Sédimentaire des Environments Littoraux dominés par la Houle," Institut de Méchanique de Grenoble, Université de Grenoble, Ph.D. Thesis, 1988.

[52] B. Boczar-Karakiewicz, D. L. Forbes & G. Drapeau, "Formation and Stability of Nearshore Bars in the Southern Gulf of St. Lawrence," *Geological Survey of Canada, Contribution 33187* (1990).

[53] I. A. Svendsen, "A Model for Sedimentary Motion under Waves," *Internal Research Note* (1977).

[54] L.T. Biegler, J. Nocedal & C. Schmid, "Reduced Hessian Methods for Large-scale Constrained Optimization, Working Paper,," Northwestern University , 1991.

[55] J. L. Bona, Personal Communication.

[56] Cz. Druet, S. R. Massel & R. Zeidel, "The Structure of Wind Waves in the Southern Baltic Sea," *Ruzprawy Hydrotechniczne* 30 (1972), 312–318.